Optimization of a φC31 integrase-controlled genetic memory switch in *Nicotiana benthamiana*

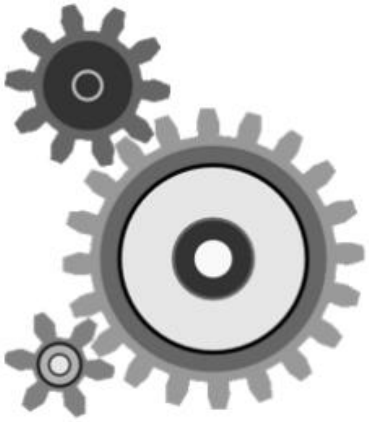

Plant Molecular and Cellular Biotechnology
Master's Thesis 2021-2022

Antonio Corbalán Acedo

Directors:

Silvia Gianoglio
Rubén Mateos Fernández
Diego Orzáez Calatayud

AGRADECIMIENTOS

Durante este año y medio he aprendido que el esfuerzo y sobre todo las ganas por cumplir tus sueños, al final dan sus frutos. Tras todo este tiempo puedo por fin decir que he acabado mi Trabajo de Fin de Máster sobre el interruptor de genes. Durante este período de mi vida en Valencia he conocido a gente maravillosa, que me han acompañado a lo largo de esta nueva etapa científica. Tanto a los que llegaron hace poco, como a los que llevan toda la vida, gracias por formar parte de la persona en la que me he convertido a día de hoy.

En primer lugar, me gustaría agradecer a mi familia su apoyo incondicional durante todos estos años. Sin ellos no estaría donde estoy, ni habría logrado todo lo que me he propuesto. Gracias mamá, porque no tengo vida para agradecerte todo lo que has hecho y das por mí.

A mis compañeros de Máster, que más que compañeros se han convertido en familia. Gracias a cada uno de vosotros por hacer que este año haya sido increíble, gracias por cada momento imborrable, por compartir alegrías y penas, nervios e inquietudes y metas y ambiciones futuras. Esto solo acaba de empezar…

A Diego Orzáez, alguien a quien admiraba en la carrera y sigo admirando. Gracias por recibirme con los brazos abiertos en el laboratorio 2.09, por darme la oportunidad de haber podido disfrutar de la Biología Sintética como lo he hecho y de haber aprendido tanto en relativamente tan poco tiempo, gracias por tu cercanía dentro y fuera del lab, por tu humildad y por todos tus consejos siempre que lo he necesitado. Ha sido un orgullo haberte tenido como jefe de laboratorio.

A mi otra “pequeña” familia italo-española, la de los labs 2.09 y 2.10, grandes científicos y científicas con quienes he aprendido y compartido grandes momentos y quienes han hecho que me sintiera como en casa. A Sara, gracias por enseñarme cómo se hacen las qRT-PCRs, por toda tu ayuda desinteresada en el laboratorio, por tu paciencia, por tus sabios consejos científicos. Te deseo lo mejor en tu nueva etapa en Bélgica, aunque estoy seguro de que te irá genial. A Asier, por dar vida al laboratorio 2.09, a todas las comidas del IBMCP y a cualquier bar al que vayamos. Gracias por tu cercanía y ayuda. A Nuccio, por tu apoyo en el lab, por escucharme y aconsejarme en algún que otro café de tarde y con alguna que otra cerveza. A Bea, gracias por encargarte de organizar todos los eventos sociales del laboratorio, porque sin ti, a ver quién queda. Gracias por lo bien que me has tratado, por tu ayuda y simpatía, por tus historias en Tanzania y por todos los momentos en los cafés

diarios de mañana y de tarde. A Marta y Elena Moreno, gracias por darme siempre vuestros sabios puntos de vista en mis experimentos con el interruptor, y por estar ahí cuando lo he necesitado sin pedir nada a cambio. Sin vosotras, no habría podido hacer muchos de mis experimentos. A Asun, gracias por responder siempre todas mis dudas científicas y por echarme un cable cuando estaba agobiado buscando doctorados. A Elena García, gracias por transmitirme tu alegría y optimismo, a pesar de que no fuera un buen día. A Jordi, gracias por tu cercanía, por preocuparte siempre y por alegrarme cuando tenía un día difícil. Espero que algún día visites Elche y yo visitar el Pirineo. A María Lobato, gracias por tus regalos del amigo invisible, muy acertados, y por resolver mis dudas de las becas y del lab. A Camilo, gracias por ayudarme con mis experimentos del TFM, ya haya sido dejándome glicerinados de bacterias o enseñándome a usar Graphpad, gran herramienta por cierto. A Víctor, porque aunque no estés mucho por el lab, hemos pasado buenos ratos fuera. A Ciro, que aunque ya estés en Italia, ha sido un placer compartir buenos ratos contigo. Ojalá algún día nos volvamos a ver. A Danilo, mi compañero incondicional de laboratorio, el que me ha ayudado a hacer muchos experimentos, y el que ha estado siempre que lo he necesitado. Nos volveremos a ver amigo mío, gracias por todo. A Silvia Presa, por mantener ambos laboratorios en orden, porque si no, reinaría el caos, gracias. Y no podía faltar, agradecer a mis tutores Silvia y Rubén, que más que tutores de TFM se han convertido en amigos y en confidentes en muchas ocasiones. Gracias de corazón por enseñarme tantísimo, por transmitirme vuestra pasión por la ciencia, por vuestra paciencia infinita y por todos los momentos vividos, y por estar a mi lado constantemente durante este año y medio, desde el primer día hasta el último. Siempre me tendréis a vuestra disposición. Por último, gracias a ti Anni, por ser mi mayor apoyo, por quererme como me quieres y por levantarme siempre que me caigo. Qué afortunado soy.

INDEX

I.- ABSTRACT

Plant synthetic biology is a young and constantly growing field of science that offers to society a wide variety of genetic tools to modify and to harness plant metabolic complexity for human benefit. To date, several genetic tools have been developed and implemented in plant systems for its use in future agriculture issues. One fascinating example is the development of the φC31 integrase-controlled genetic memory switch, which allows to transcriptionally regulate the activation of any two genes of interest by simply using a recombinase protein from phage φC31. Other alluring plant genetic devices are the dCas9-based gene regulators, which take advantage of dCas9 protein variant that can bind target DNA sequences but not cleave them. By fusing transcriptional activators or repressors to these dCas9 proteins and using the appropriate RNA guides it is able to regulate the expression of any gene of interest. In the present research of Master‘s thesis, we have optimized the φC31 integrase protein dose necessary for the optimal switch activation, using two transgenic *Nicotiana benthamiana* plant lines carrying different switch constructs. In these lines, we transiently expressed the φC31 integrase under different conditions, testing four promoters of growing strengths and three *Agrobacterium tumefaciens* optical densities (OD_{600}), with the aim of finding out the optimal conditions for integrase expression and subsequent switch activation. Once the optimals conditions were set, we designed two new memory switches that combined switch device architecture with the regulatory potential of a dCas9-based transcriptional activation system called dCasEV2.1. Regulating dCasEV2.1 system through switch tool overcame the limit of controlling just two genes of interest and allowed us to regulate different downstream genes by choosing an appropriate RNA guide. New switch versions were functionally characterized in *N. benthamiana* WT plants by transient expression and subsequent molecular assays including bioluminiscence and fluorescence assays, analysis of gene expression through quantitative RT-PCR or analysis of volatile Lepidopteran sex pheromones by GC-MS.

Key Words: memory switch; φC31 integrase; *att sites*; dCas9-based regulation; synthetic biology; synthetic tools; *Nicotiana benthamiana*; plant biotechnology; metabolic engineering; moth sex pheromones

Abbreviations

DNA: deoxyribonucleic acid

RNA: ribonucleic acid

gDNA: genomic DNA

cDNA: complementary DNA

T-DNA: Tranfer-DNA

REs: Restriction Enzymes

GB: GoldenBraid

pUPD2: Universal Parts Domesticator plasmid 2

pDGB3: Destination GoldenBraid plasmid 3

PCR: Polymerase Chain Reaction

qRT-PCR: Real-Time Quantitative Reverse Transcription PCR

***RL*:** *attR* and *attL* sites

PB: *attP* and *attB* sites

PR: Promoter

CDS: Coding Sequence

TM: Terminator

TU: Transcriptional Unit

CRISPR: Clustered Regularly Interspaced Short Palindromic Repeats

Cas: CRISPR associated

PAM: Protospacer-Adjacent Motif

dCas9: dead Cas9

DSB: Double-Stranded Break

sgRNA: single-guide RNA

crRNA: CRISPR RNA

tracrRNA: *trans*-activating crRNA

dCasEV2.1: dead Cas9-EDLL + MS2-VPR + gRNA2.1

IPTG: isopropyl β-d-1-thiogalactopyranoside

X-gal: 5-bromo-4-chloro-3-indolyl-β-D-galactopyranoside

BSA: Bovine Serum Albumin

WT: Wild Type

MS media: Murashige & Skoog media

dpi: days post infiltration

LB medium: Luria-Bertani medium

***YFP*:** Yellow Fluorescent Protein gene

Luc: Luciferase gene

Fluc: Firefly luciferase

Rluc: Renilla luciferase

approx.: approximately

OD_{600}: Optical Density measured at 600 nm

NHGRI: National Human Genome Research Institute

SynBio: Synthetic Biology

GOI: Gene of Interest

RDF: Recombination Directionality Factor

CaMV: Cauliflower Mosaic Virus

NHEJ: Non-Homologous End Joining

HR: Homologous Recombination

SNP: Single Nucleotide Polymorphism

scFv: single-chain variable fragment

Rta: R transactivator

CRISPRa: CRISPR-mediated activation

CRISPRi: CRISPR-mediated interference

VPR: VP64-p65AD-Rta activation domains fusion

TV: TALE-VP64 activation domains fusion

MS2: phage MS2 coat protein

PhiC31R: PhiC31 recombinase

R2 line: Register 2 line

R4 line: Register 4 line

Oligo: Oligonucleotide

SD: Standard Deviation

GC-MS: Gas chromatography–Mass spectrometry

SF: Stuffer Fragment (empty vector)

a.u.: arbitrary un

II.- INTRODUCTION

II.1.- Synthetic biology beginnings and fundamentals

The idea of modifying organisms to obtain products of human interest is probably as old as civilization, but the technology to accomplish this goal in a specific, directed manner started to be developed just some decades ago, between the 1970s and 1980s, with the development of DNA manipulation and cloning tools, polymerase chain reaction (PCR) and DNA sequencing techniques. Nevertheless, during this period, genetic engineering approaches were not equipped with the necessary knowledge or tools to create biological systems which display the diversity and depth of regulatory behaviour found in complex organisms such as plants (Cameron et al., 2014). It was in the mid-1990s, in concomitance with the emergence of powerful computational tools and high-throughput molecular techniques, when biologists and computer scientists began to collaborate to generate vast quantities of 'omics' data (genomic, transcriptomic, proteomic or metabolomic, among others) that would help gain a deeper understanding of the complexity of cellular networks. This new knowledge allowed the genetic redesign of biological systems, with breakthrough achievements such as the first synthetic gene-regulatory circuits in the bacterium *Escherichia coli*, the toggle switch (Gardner et al., 2000) and the 'repressilator' (Elowitz & Leibler, 2000), or such as the design of new molecular pathways, like the first synthetic MAP kinase pathway in the yeast *Saccharomyces cerevisiae* (Park et al., 2003). These early genetic circuits constitute the starting point of the currently expanding research branch called Synthetic Biology (SynBio), that according to the National Human Genome Research Institute (NHGRI; https://www.genome.gov/about-genomics/policy-issues/Synthetic-Biology) is defined as: "*A field of science that involves redesigning organisms for useful purposes by engineering them to have new abilities, in which researchers and companies around the world are harnessing the power of nature to solve problems in medicine, manufacturing and agriculture*"

SynBio combines the engineering principles of standardization, modularity, and abstraction of function with organisms' biology (Way et al., 2014; Liu & Stewart, 2015; Bernabé-Orts et al., 2020; Garner, 2021), either to provide organisms with new traits (top-down approaches, in which organisms are considered as chassis) or to create from basic components new biological systems which do not exist in nature

(bottom-up approaches). In contrast with 'traditional' engineers, synthetic biologists use DNA molecules as building blocks, which can eventually be combined into artificial living systems. This building process generally follows iterative cycles of Design, Build, Test and Learn. In the Design stage, a genetic part or system is sketched *in silico*. Next, in the Build stage, the computer model is assembled through genetic engineering and cloning tools for its subsequent functional characterization (Test stage). Finally, in the Learn step, the system provides information and knowledge that can be used to refine and improve the performance of the initial model (a new Design step). After a number of iterative cycles, the desired new trait, function or biological system is achieved (Garner, 2021).

II.2.- Plant synthetic biology

Since the emergence of the SynBio era, research in this field has been focused on microbial systems, being *E. coli* and *S. cerevisiae* the most used models. Recently, interest focused on mammalian cells, such as in the case of the use of re-engineered T lymphocytes for the treatment of ALL leukaemia (Garner, 2021), or the production of RNA- and cell-based vaccines (Liu & Stewart, 2015). Despite all scientific progress on these organisms, synthetic biology has hardly exploited plant systems. Plants constitute the most important source of primary metabolites (proteins, fatty acids, and carbohydrates), which are essential to human and animal diets, and they also display a wide variety of secondary metabolites that are highly valuable in medicine, agriculture, and industry. Thus, their complex metabolism makes them ideal chassis that can be harnessed to produce all type of molecules. Further, there are some features that make plants excellent systems for SynBio approaches: (i) they are safer biofactories, since the risk of contamination with human pathogens is minimum (Mett et al., 2008); (ii) their nutritional requirements can be fulfilled with abundant and cheap resources, since they basically need carbon dioxide, water and sunlight; (iii) they are not subject to ethical questions, which sometimes limit the use of animal cells; (iv) the SynBio principles and concepts developed in microbial systems are often applicable to plants, and some bacterial genetic devices can be directly transferred to them, enhancing the design and construction of novel plant functions (Baltes & Voytas, 2015; Liu & Stewart, 2015).

To date, plant SynBio projects range from creating new metabolic pathways for producing added-value metabolites, to designing plant synthetic regulatory tools

as genetic switches or CRISPR/Cas-based tools, to ambitious projects which aim to integrate a new entire metabolism into species of agronomical interest.

II.2.1- Synthetic metabolic pathways

Currently, the potential of plant metabolic complexity has not been exploited as much as it could be. Market demand of recombinant proteins and valuable metabolites is continuously growing: that is why the implementation of new synthetic metabolic pathways in plant systems is needed. An example of the introduction of a synthetic metabolic pathway in plants is the transformation of the genes for the biosynthesis of the cyanogenic glycoside dhurrin from sorghum (*Sorghum bicolor*) into *Nicotiana benthamina*, where chloroplast-specific production of dhurrin was achieved (Nielsen et al., 2013), and in *Arabidopsis thaliana* (Kristensen et al., 2005), where dhurrin production reached 4% dry-weight. Recently, *N. benthamiana* was stably transformed with three pheromone biosynthetic genes, the *Amyelois transitella AtrΔ11* desaturase gene, the *Helicoverpa armigera* fatty acyl reductase *HarFAR* gene, and the *Euonymus alatus* diacylglycerol acetyltransferase *EaDAct* gene (Mateos-Fernández et al., 2021). As a result, plants were able to produce (*Z*)-11-hexadecenol (Z11-16OH) and (*Z*)-11-hexadecenyl acetate (Z11-16OAc), two volatile moth sex pheromones produced by many Lepidoptera. This innovative strategy opens a sustainable alternative to control pests in agriculture.

Plant SynBio has also given rise to projects for plant vitamin fortification (biofortification) in crops of agronomical interest, as reported by Diretto et al. (2007), who expressed three *Erwinia* bacterial genes (*CrtB*, *CrtI* and *CrtY*) under tuber-specific promoter control in potato (*Solanum tuberosum*), which resulted in tubers containing high carotenoid levels, with a 3600-fold increase of β-carotene (provitamin A) and approx. a 20-fold increase of other carotenoids with respect to WT potatoes; or by Storozhenko et al. (2007), who obtained transgenic rice (*Oryza sativa*) through the endosperm-specific overexpression of two *A. thaliana* genes (*GTPCHI8* and *ADCS9*) of the folate biosynthetic pathway, resulting in rice grains enriched in folate (vitamin B9), that contained up to four times the adult daily folate requirement per each 100 g.

Other plant SynBio strategies involve ambitious objectives as the reprogramming of entire metabolisms. One example is the C4 rice project, which aims to identify and engineer the genes necessary to install C4 photosynthesis in rice, which has a C3 metabolism. The conversion of the C3 photosynthesis pathway

into C4 will increase the photosynthetic capacity of rice, consequently increasing yield (von Caemmerer et al., 2012). Another challenging project is the development of nitrogen-fixing cereals. The uptake of atmospheric nitrogen can be achieved either by introducing the signalling pathway for rhizobia symbiosis from legumes or by engineering the expression of the nitrogenase enzymatic complex into cereal crops (Oldroyd & Dixon, 2014). These crops will reduce the dependency on inorganic fertilizers as nitrate and ammonium, thus producing sustainable and higher-yielding cereals.

II.2.2- Synthetic regulatory genetic switches

Synthetic switches are DNA constructs which have been engineered in a modular way, following SynBio principles. As occurs in natural molecular networks, genetic switches can integrate input signals, for instance a chemical or an environmental signal, and they are able to generate an output response. In plants, this can be the specific control over agronomically-relevant processes such as flowering time, metabolite or protein production or even abiotic and biotic stress responses (Bernabé-Orts et al., 2020). When genetic switches are integrated in living organisms, different parameters must be taken into consideration for their optimal performance, since the final behaviour does not always fit with the expected outcome. First, a deep functional characterization and a solid mathematical model of a switch module is fundamental. Second, the orthogonality of switch components is also essential, to avoid undesired interactions with endogenous plant networks, which could compromise switch functionality. Finally, a series of functional parameters must be studied, including the switch dynamic range (ratio between maximum and basal activation levels), leakiness (basal switch activity without inducing activation signal), kinetics or reversibility of its function (Andres et al., 2019). Most of the regulatory switch tools created to date depend on the constant addition of activators or repressors to sustain the desired cellular outputs. Generally, switch input signals are chemical substances such as ethanol (Caddick et al., 1998; Roberts et al., 2005), β-estradiol (Böhmdorfer et al., 2010), glucocorticoids such as dexamethasone (Aoyama & Chua, 1997), copper (Saijo & Nagasawa, 2014) or antibiotics such as tetracycline (Weinmann et al., 1994). However, chemical-inducible switches have several limitations concerning the high cost of chemical inducers, their challenging administration in large crop fields, their diffusion that does not allow defined spatiotemporal activation, and their possible toxic effect on the

environment. In addition, these switch devices lack long-term and heritable memory storage. Recently, light-controlled genetic switches have been developed and implemented in plants, giving rise to a new but growing research field called optogenetics. New light-controlled versions include a phytochrome-based red light-inducible system (PhyB/PIF6), which is activated by red light (660 nm) that induces PhyB-PIF6 heterodimerization and subsequent reporter gene expression, and inactivated by far-red light (740 nm), which dissociates the complex (Müller et al., 2014); and a bacterial photoreceptor CarH-based green light-regulated expression system (CarH/CarO), in which green light deactivates gene expression (Chatelle et al., 2018). Light-regulated switches overcame most of the chemical-inducible switches' drawbacks, but long-term and heritable genetic memory was still absent.

Last year, the first reversible memory switch for whole plant systems was published, which is based on the activity of the *Streptomyces* bacteriophage φC31 serine integrase and its cognate recombination directionality factor, RDF (Bernabé-Orts et al., 2020). The switch system is formed by a central invertible element, which contains the CaMV 35S promoter and the Mtb terminator sequences, flanked by two opposite site-specific recombination sites (*attP* and *attB*), to control the transcription of two genes of interest (*GOIs*). The switch has an initial state, named as *PB* configuration, where the *GOI* located at the right side of the device is transcriptionally active (ON mode), while the *GOI* on the left remains inactive (OFF mode). When the φC31 recombinase is added to the system, it can catalyse the recombination of *attP* and *attB* DNA sites generating hybrid *attR* and *attL* sites in a unidirectional reaction (Grindley et al., 2006; Smith et al., 2010), consequently changing the *PB* configuration of the switch to the *RL* state. This reaction is defined as the SET operation (Figure 1) and involves the genomic re-arrangement by inversion of the central regulatory element, the transcriptional activation of the left *GOI* (OFF→ON) and the inactivation of the initial activated *GOI* on the right (ON→OFF). The new *RL* status is maintained over time (long-term and heritable genetic memory) until intentionally reversed to the *PB* state, in the RESET operation, through the combined supply of the φC31 serine integrase and an allosteric modulator of its activity, the RDF factor (Khaleel et al., 2011).

In this work, we will refer to switch DNA constructs as *PB GOI1*:*GOI2* or as *RL GOI1*:*GOI2*, where the state of the switch is denoted by the letters *PB* or *RL* indicating the configuration of the *att* recombination sites, and the active gene of interest (*GOI1* or *GOI2*) is underlined.

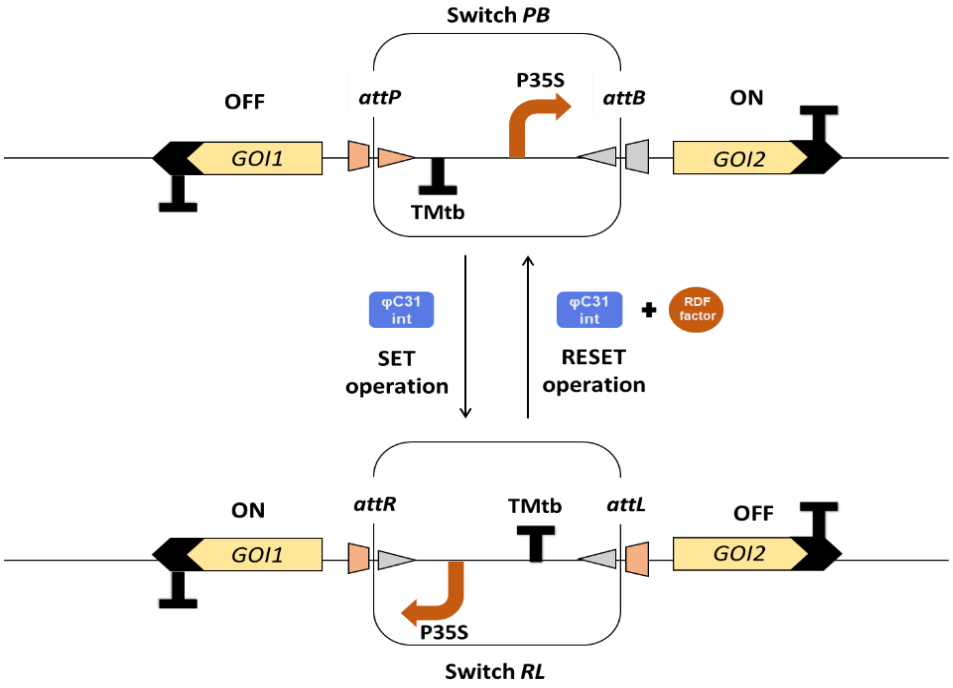

Figure 1.- Representation of φC31-based memory switch device for plant systems. A central genetic invertible element containing the CaMV 35S promoter (P35S) and the Mtb terminator (TMtb) works as a switch, regulating the expression of two genes of interest (*GOI1* and *GOI2*). When the phage φC31 integrase (φC31 int) is supplied, it catalyses site-specific recombination of the *attP* and *attB* sites flanking the central invertible element, creating the chimeric *attR* and *attL* sites (SET operation). This event results in a genomic inversion of the central regulatory element that changes expression states of both *GOI*, transcriptionally activating the *GOI1* (ON) and inactivating *GOI2* (OFF). This genetic configuration can be reversed by expressing the φC31 recombinase together with a recombination directionality factor (RDF), which both catalyse the recombination of *attR* and *attL* sites and reset the switch to its original state (RESET operation).

II.3.- From CRISPR/Cas bacterial defence systems to CRISPR/Cas-based genetic tools in plants

Since the publication of the bacterial CRISPR/Cas adaptative immune systems (Mojica et al., 2005; Barrangou et al., 2007) as potential genome editing tools (Jinek et al., 2012), many types of CRISPR/Cas-based genetic regulation tools have been developed and extensively used so far.

II.3.1.- Natural CRISPR/Cas systems

Clustered regularly interspaced short palindromic repeats (CRISPR) and CRISPR associated proteins (Cas), constituting CRISPR/Cas systems, are natural defence tools used by bacterial and archaeal species to fend off invading phages

and foreign genetic elements. Briefly, when a phage infects a bacterial host equipped with a CRISPR system, the bacterium acquires several phage DNA fragments and incorporates them into its genomic CRISPR arrays in a process called adaptation phase. Next, in the biogenesis phase, CRISPR sequences are transcribed and processed into mature RNAs called crRNAs. Finally, in the immunity phase, Cas proteins use these crRNAs, which are complementary to the phage sequences, as guides to target the phage genome during subsequent invasions; once the Cas-crRNA complex is positioned on its target sequence, Cas nucleases cleave phage DNA, consequently eliminating phage infection (Sedeek et al., 2019a). In the case of the *Streptococcus pyogenes* CRISPR/Cas system, the Cas protein is the Cas9 nuclease that binds to two different RNAs (the guide crRNA and a *trans*-activating RNA (tracrRNA), necessary for crRNA maturation (Deltcheva et al., 2011)) to target a specific DNA sequence and cut it through a double-stranded break (DSB), three nucleotides upstream a specific DNA motif called PAM (protospacer-adjacent motif). Cas9 HNH nuclease domain cleaves the complementary strand to the cRNA while the Cas9 RuvC-like domain cleaves the noncomplementary strand (Jinek et al., 2012).

II.3.2.- CRISPR/Cas as gene editing tool

In 2012, breakthrough research changed genome editing forever. (Jinek et al., 2012) modified the *S. pyogenes* CRISPR/Cas9 system by fusing crRNA and tracrRNA into a unique RNA called single-guide RNA (sgRNA). The sgRNA comprised an invariable RNA scaffold and a variable and programmable RNA guide which could be targeted to any DNA sequence, thus, being a potential tool for the gene editing of any organism. This was first demonstrated *in vivo* by Jiang et al. (2013), who successfully introduced precise mutations in the genomes of *Streptococcus pneumoniae* and *E. coli* using the CRISPR/Cas9 system and specific sgRNAs. Since then, CRISPR/Cas9 efficiency and precision have been demonstrated in many other organisms, including plants. CRISPR/Cas9 gene editing tools have been applied to plant biology models such as *A. thaliana* (Feng et al., 2018) or *N. benthamiana* (Jansing et al., 2019) or to crops of agronomical interest to obtain mutants with desired traits, such as low-gluten wheat varieties (*Triticum sp*.) (Sánchez-León et al., 2018), pink-fruited tomatoes (*Solanum lycopersicum*) (Yang et al., 2019) or eggplants (*Solanum melongena*) with reduction in flesh fruit browning (Maioli et al., 2020), among many other examples.

In all cases, CRISPR/Cas-induced mutagenesis is based on the repair mechanism that occurs after the Cas9-mediated DNA DSB. After cleavage, DNA cuts can be repaired through the Non-homologous End Joining (NHEJ) pathway or by Homologous Recombination (HR). The NHEJ pathway, which is predominant in plants, relies on the processing of the two broken DNA ends to create compatible ends that are later ligated. This process often implies the introduction of insertion/deletions of one or few nucleotides that lead to random genetic mutations, which typically cause gene loss-of-function. On the other hand, the HR pathway uses a DNA homologous sequence, which can be delivered with CRISPR machinery, to restore the DSB site. This latter can be useful if accurate genomic changes such as single nucleotide polymorphisms (SNPs) are desired (Sedeek et al., 2019b).

II.3.3- CRISPR/Cas-based gene-activating tools

In addition to gene editing, CRISPR/Cas systems have been repurposed as a programmable platform for transcriptional and post-transcriptional regulation (Pan et al., 2021). This is possible thanks to the design of dead Cas variants (dCas), which have been mutated on their nuclease domains to create catalytically inactive Cas proteins, which remain competent for RNA-guided DNA binding but inadequate to induce DNA DSBs. In the case of the dead Cas9 variant (hereinafter dCas9), this contains two silencing mutations at the RuvC1 and HNH nuclease domains (D10A and H841A) (Qi et al., 2013), thus losing its cleavage activity. The dCas proteins can be fused with effector proteins such as transcriptional activators, repressors, and epigenetic modulators, enabling efficient gene-specific CRISPR-mediated activation (CRISPRa), interference (CRISPRi), and epigenome modifications, respectively (McCarty et al., 2020). With regards to CRISPRa in plants, early approaches consisted in fusing the dCas9 C-terminus to transcriptional activation domains such as VP64, EDLL or the transcriptional activator-like (TAL) effector (Lowder et al., 2015; Piatek et al., 2015). These early systems achieved gene target upregulation, either by using one sgRNA or multiple sgRNAs targeting a gene, but activation fold changes were not much higher than a 12-fold increase.

Therefore, many different strategies were developed to enhance CRISPR/Cas-based activation in plants. The first strategy is called dCas9-SunTag and aims to recruit several copies of transcriptional activators. In this approach, several tandem repeats of a small antibody epitope (peptide GCN4) are fused to dCas9. These epitopes can interact and recruit multiple copies of a single-chain

variable fragment (scFv) fused to any transcriptional activator such as VP64, as reported in *A. thaliana* (Papikian et al., 2019). A second strategy to enhance CRISPRa potency is based on fusing various activators in tandem to dCas proteins: these include the VPR activator, an improved activation module that is composed of a hybrid tripartite activator, VP64, p65AD, and Epstein–Barr virus R transactivator (Rta). The dCas9-VPR fusion exhibited greater activation of endogenous targets than the dCas9-VP64 simple fusion (Chavez et al., 2015). Another option is the TV activator, a fusion of six copies of the TALE transcription activation domain and two copies of VP64 which, fused to dCas9 (dCas9-TV system), exhibited strong transcriptional activation of single or multiple target genes in rice and *Arabidopsis* (Li et al., 2017). A third approach consists of using sgRNA scaffolds to recruit activation domains (Zalatan et al., 2015), which can act synergistically in enhancing endogenous gene activation. One notable example is the sgRNA2.0 scaffold designed by Konermann et al. (2015), a modified sgRNA that contains two copies of a MS2-binding RNA hairpin that can specifically bind two coat proteins from the MS2 bacteriophage which, fused to transcriptional activation domains such as VP64 (MS2-VP64), can enhance gene activation. The recruitment of MS2-VP64 fusions by MS2-binding RNA hairpins in sgRNA2.0 systems resulted in an additive effect, leading to a 12-fold increase in *Neurog2* gene activation over the dCas9-VP64 fusion activation system (Konermann et al., 2015). Combining these strategies, Selma et al. (2019) designed a potent CRISPR/Cas-based programmable transcriptional activator. This genetic tool comprised dCas9 fused with the EDLL activation domain (dCas9-EDLL) and a novel sgRNA2.1 that can recruit MS2-VPR fusions by binding to MS2-binding RNA hairpins. This combination was named as dCasEV2.1 (Figure 2) and was shown to induce, following a multiplexing strategy in which several gRNAs are combined (Xie et al., 2015), activation rates of 10,000-fold and 4,000-fold when targeting the *NbDFR* and *NbAN2 N. benthamiana* endogenous genes, respectively (Selma et al., 2019)**.**

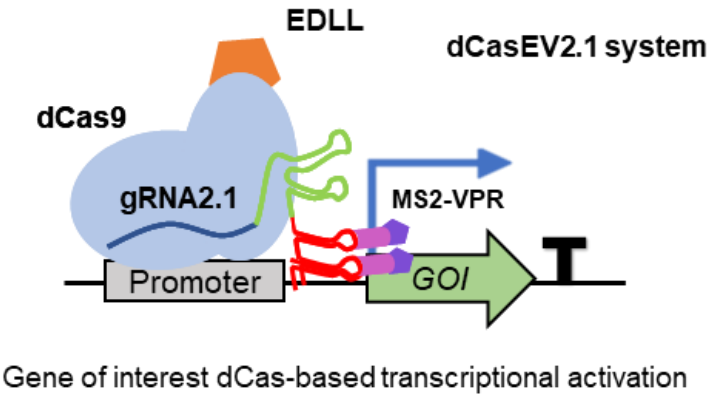

Figure 2.- Schema of the dCasEV2.1 transcriptional activation system. This potent gene-activating tool consists of a dCas9 protein fused to EDLL activation domain (dCas9-EDLL), a programmable RNA guide (gRNA2.1) and hybrid tripartite activators VPR fused to MS2 phage coat protein (MS2-VPR), which are bound to gRNA2.1 harpins through MS2-anchoring RNA sites. Once the complex binds its target sequence through gRNA-mediated recognition, activator proteins (EDLL and VPR) can interact with plant cell transcriptional machinery and consequently transcriptionally activate *GOIs*.

II.4.- Combining regulatory approaches for the fine-tuning of gene expression in plants.

In this Master's thesis we have combined the SynBio principles of standardization, modularity and abstraction to create new memory switch devices that regulate the expression of the dCasEV2.1 transcriptional activation system. These new dCasEV2.1-based switch versions, together with the delivery of appropriate gRNAs, would enable us to induce the expression of any selected downstream target genes. Combining both plant synthetic tools, the memory switch and the dCasEV2.1 activation system, would overcome the limit of controlling just two genes of interest and would allow to precisely control multiple genetic pathways by simply choosing the right gRNA combination. One alluring application we are especially interested in is the production of moth sex pheromones in plants. These added-value compounds have been successfully produced in *N. benthamiana* transgenic plants, as reported by Mateos-Fernández et al. (2021), but their accumulation in the early development stages caused toxicity and growth penalties, resulting in a dwarf phenotype. Thus, using the switch to activate the dCasEV2.1 tool to control moth pheromone production in a customizable way in fully developed *N. benthamiana* plants is an appealing solution to avoid pheromone toxicity and consequently increase product yield.

III.- OBJECTIVES

The general goal of this Master's thesis is to optimize the activation of a plant molecular switch based on the phage φC31 integration system recently characterized by Bernabé-Orts et al. (2020). To do so, the following specific objectives will be set:

1. To characterize, in two *N. benthamiana* transgenic lines, *PB Luc:YFP* (GB1643; R2) and *PB YFP:Luc* (GB1644; R4), the dose-dependent activation of gene expression (SET operation) by means of agroinfiltration of the φC31 recombinase. For this purpose, two parameters will be studied:
    a. The influence of promoter strength on φC31 integrase gene expression and subsequent switch-mediated gene activation, testing four promoters: P35S, PNos, PNtA1 and PNtA11
    b. The influence of *Agrobacterium tumefaciens* optical density (OD_{600}), assaying three different ODs: 0.1 / 0.01 / 0.001
2. Once the optimal conditions for switch-mediated gene activation are set, to design and characterize two new dCasEV2.1-based genetic switches (*PB dCas9-EDLL:Luc* and *PB dCas9-EDLL:YFP*) for the control of different downstream pathways. For this objective, different experiments will be carried out:
    a. Testing of the functionality of the new switches by *Agrobacterium*-mediated transient expression, using the optimized conditions determined before
    b. Confocal laser microscopy to determine the expression of the YFP reporter controlled by the switch
    c. Bioluminiscence assays to determine the levels of the Luc reporter directly controlled by the switch
    d. Bioluminiscence assays to determine the levels of a downstream Luc reporter activated by the dCasEV2.1 system
    e. GC-MS to analyse the dCasEV2.1-induced production of Lepidopteran sex pheromones
    f. Quantitative RT-PCRs to determine the transcript levels of the genes regulated by the switch

IV.- MATERIALS AND METHODS

IV.1- GoldenBraid Cloning Technology

All the constructs used in this Master's thesis were assembled using the GoldenBraid assembly platform, available at https://gbcloning.upv.es/. GoldenBraid is a modular and iterative DNA assembly system (Sarrion-Perdigones et al., 2014) based on the Golden Gate cloning strategy which uses type IIS REs, in particular *Bsa*I and *Bsm*BI, to generate DNA fragments with compatible overhangs, which are later assembled in specific GB vectors thanks to a T4 ligase. In the GoldenBraid system, the cloning process of any DNA fragment starts with its domestication. This process involves the adaptation of a DNA sequence (so-called GB part) to the GoldenBraid grammar, either by PCR amplification using GB-adapted primers or by DNA synthesis. Additionally, the domestication step involves the removal of internal *Bsa*I or *Bsm*BI restriction sites through the introduction of synonymous substitutions, to avoid internal digestion of the DNA sequences of interest.

Next, domesticated DNA parts are cloned into standard entry pUPD2 vectors (Vazquez-Vilar et al., 2017a), through a *Bsm*BI-mediated restriction-ligation reaction, comprising Level 0 assemblies which include DNA sequences such as promoters (PR), coding sequences (CDS) or terminators (TM). In addition, pUPD2 vectors incorporate *Bsa*I sites flanking GB Level 0 parts, which allow to release domesticated DNA pieces and clone them together into destination plasmids called pDGB3, to create Level 1 GB elements, typically a full transcriptional unit (TU) (Sarrion-Perdigones et al., 2013). There are four destination plasmids which are classified into two other levels, level α (pDGB3 α1 and pDGB3 α2) and level Ω (pDGB3 Ω1 and pDGB3 Ω2). pDGB3 plasmids are binary vectors that contain a GB cassette (a selection *LacZ* gene) flanked by two restriction sites for *Bsa*I and for *Bsm*BI, but the position and orientation of these sites differ between the two levels. Moreover, pDGB3 α vectors include kanamycin resistance for bacteria selection, whereas pDGB3 Ω plasmids have spectinomycin resistance (Sarrion-Perdigones et al., 2013).

Due to their binary nature, GB Level 1 elements (TUs) from α or Ω vectors can be reused and exchanged iteratively. For instance, TUs from different α plasmids in Level 1 can be assembled through a single-tube *Bsa*I digestion-ligation reaction into Level 2 Ω plasmids. Next, TUs from different Level 2 Ω plasmids can also be assembled in Level 3 α vectors in a single-tube *Bsm*BI digestion-ligation mix. This cloning process can be repeated indefinitely.

Therefore, binary assemblies allow us to develop increasingly complex multigenic constructs and design highly complex biological new functions in plants.

IV.1.1- DNA sequences amplification and synthesis

All DNA GB Level 0 parts employed in this thesis were already domesticated and uploaded to the GoldenBraid database, except for the *dCas9-EDLL* gene included in the new switch designs of this work. The *dCas9-EDLL:TNos* sequence was amplified by PCR from plasmid GB1190 using adapted primers SGS21ABR01_Fw and SGS21ABR02_Rv (Supplementary Table 2). These primers would include specific overhangs to the amplified fragment, allowing its cloning in pUPD2 (as 1/3 assembly part) and further in pDGB3 α to create dCasEV2.1-based switches.

The set of primers for *dCas9-EDLL:TNos* amplification were generated using GoldenBraid's GB Domesticator tool (https://gbcloning.upv.es/do/domestication/) in a non-conventional way, since switch assembly parts have their own GB grammar (Supplementary Figure 1).

PCR reactions were carried out using Thermo Scientific's Phusion High-Fidelity DNA Polymerase and following the HF Buffer Protocol (Table 1).

Table 1.- PCR running program for *dCas9-EDLL:TNos* amplification

Cycle Step	Temperature	Time	Cycles
Initial Denaturation	98ºC	30 s	1
Denaturation	98ºC	10 s	30
Annealing	62.3ºC	20 s	
Extension	72ºC	2.5 min (30 s/kb)	
Final Extension	72ºC	10 min	1
Hold	4ºC	Hold	Hold

IV.1.2- GoldenBraid parts assembly

For domesticated DNA linear sequences, an amount of 60 fmol was cloned into 20 fmol of a pUPD2 destination plasmid through a *Bsm*BI-mediated restriction-ligation reaction to create Level 0 GB parts as described by Engler et al. (2008) and Sarrion-Perdigones et al. (2011) (Table 2).

Table 2.- Level 0 restriction-ligation reagents and amounts.

Reaction component	Amount
PCR fragment/synthetic DNA insert	60 fmol
pUPD2 destination plasmid	20 fmol
T4 DNA Ligase Buffer x10	1.5 µL
T4 DNA Ligase (200 U/µL)	1 µL
BSA (1mg/mL)	1.5 µL
*Bsm*BI enzyme (5 U/µL)	0.8 µL
H_20	Up to 15 µL

Subsequently, Level 1 assemblies were performed by cloning 40 fmol of each Level 0 GB part - such as PR (promoter), CDS (coding sequence) or TM (terminator) - contained in pUPD2 vectors into 20 fmol of a pDGB3 α destination plasmid by a multipartite *Bsa*I-mediated cloning reaction (Table 3) to obtain a TU.

Table 3.- Level 1 multipartite assembly components and amounts.

Reaction component	Amount
pUPD2_PR plasmid	40 fmol
pUPD2_CDS plasmid	40 fmol
pUPD2_TM plasmid	40 fmol
pDGB3 α destination vector	20 fmol
T4 DNA Ligase Buffer x10	1.5 µL
T4 DNA Ligase (200 U/µL)	1 µL
BSA (1mg/mL)	1.5 µL
*Bsa*I enzyme (5 U/µL)	0.8 µL
H_20	Up to 15 µL

Finally, when necessary, Level 1 parts (TUs) were binary-assembled in Level 2 Ω destination plasmids through a *Bsm*BI-mediated reaction (Table 4) to create new modules.

All reactions were incubated in a thermocycler during 25- or 50- cycle digestion/ligation reactions (2 min at 37°C, 5 min at 16°C) depending on assembly complexity.

Table 4.- Level 2 binary assembly components and amounts.

Reaction component	Amount
pDGB3 α1 vector (TU1)	40 fmol
pDGB3 α2 vector (TU2)	40 fmol
pDGB3 Ω destination plasmid	20 fmol
T4 DNA Ligase Buffer x10	1.5 µL
T4 DNA Ligase (200 U/µL)	1 µL
BSA (1mg/mL)	1.5 µL
*Bsm*BI enzyme (5 U/µL)	0.8 µL
H_20	Up to 15 µL

IV.2- Plasmid multiplication in *Escherichia coli* and selection media

Ligation products were transformed into *E. coli* TOP10 competent cells for plasmid multiplication. For transformation, the ZYMO RESEARCH Mix & Go *E. coli* Transformation Kit Protocol was followed. Briefly, 1-5 µL of the digestion-ligation reaction were gently mixed with a 50-100 µL competent cells aliquot, which was incubated on ice for 3-5 minutes, followed by the addition of 300 µL of SOC medium (20 g/L tryptone, 5 g/L yeast extract, 10 mM NaCl, 2.5 mM KCl, 20 mM glucose and 10mM $MgCl_2$ and 10mM $MgSO_4$). After 1 h of shaking incubation at 37°C, transformed cells were plated onto solid LB (5 g/L yeast extract, tryptone 10 g/L and 10 g/L NaCl) agar plates containing the appropriate antibiotic (based on destination vector resistance), 40 mg/L X-gal and 0.4 mM IPTG for blue/white colony screening, and they were grown at 37°C overnight.

When assemblies were performed using pUPD2 destination vectors, white colonies were selected in solid LB medium supplemented with the antibiotic chloramphenicol (34 mg/L), while when pDGB3 α and pDGB3 Ω acceptor plasmids were used, white colonies were selected in solid LB agar medium with kanamycin (50 mg/L) or spectinomycin (50 mg/L), respectively.

IV.3- Plasmid purification and validation

To purify plasmids of interest, *E. coli* white colonies were isolated with a plastic bacterial inoculating loop and inoculated into 4 mL of liquid LB culture media supplemented with the corresponding antibiotic. Cells were grown at 37°C in agitation overnight. DNA plasmid isolation was carried out using the Omega Bio-

Tek's E.Z.N.A. Plasmid Mini Kit I, following the manufacturer's instructions and DNA concentration was measured making use of Thermo Scientific™ NanoDrop 2000c Spectrophotometer. Finally, plasmids were validated and confirmed by digestion reactions (Table 5), incubated with restriction enzymes for 1 h at 37°C, and then the resulting band patterns were visualized and analysed on a 1% agarose gel stained with Ethidium bromide.

Table 5.- Standard digestion mix for plasmid validation

Reagent	Volume (µL)
Enzyme Buffer x 10	2
Restriction enzyme (RE)	0.5
H_2O	15.5
DNA plasmid miniprep	2

All DNA sequences cloned in pUPD2 vectors, coming from PCR products or chemically synthesized DNA fragments, were sequenced by Sanger sequencing as an additional validation step.

IV.4- Bacterial glycerol stocks and GoldenBraid collection

500 µL of saturated liquid culture from previously verified colonies were mixed with 500 µL of glycerol 50% and stored at -80°C for their cryopreservation. Next, generated GB sequences were given an ID and uploaded to the GoldenBraid registry (https://gbcloning.upv.es/). All plasmids used in this work are listed in Supplementary Table 1.

IV.5- *Agrobacterium tumefaciens* transformation

Plasmids for plant expression were transferred to *A. tumefaciens* cells. In this work, the *A. tumefaciens* C58 strain was used, due to its capacity to introduce its T-DNA into infected plant cells in transient expression assays. 100-200 ng of purified DNA plasmids were mixed with 50 µL of *A. tumefaciens* C58 electrocompetent cell aliquots prepared in the lab and transferred to a cold electroporation cuvette. A 1440 V/cm electroporation pulse was applied to the cells, followed by the addition of 500 µL of SOC medium to recover electroporated bacteria. Cell suspension was grown at 28°C in a shaking incubator for 2 h. Next, 50 µL of the incubated cell suspension

were plated onto LB agar plates containing the corresponding plasmid selection antibiotic and 50 mg/mL rifampicin, which selects the C58 strain. Plates were grown at 28°C for 48 h. Colonies were then isolated onto 5 mL of LB media containing rifampicin and the corresponding antibiotic. After another 48 h-incubation step at 28°C, plasmid isolation was performed using QIAGEN's QIAPrep Spin Miniprep Kit, that yields a higher plasmid purification efficiency than Omega Bio-Tek's E.Z.N.A. Plasmid Mini Kit I. Finally, isolated plasmids were verified by restriction assays as previously described.

IV.6- *Nicotiana benthamiana* seed sterilization and viral disinfection

A volume of 50 µL of wild type (WT) or transgenic seeds were transferred into a 1.5 mL sterile Eppendorf tube and mixed with 2 mL of 10% TPS (Trisodium phosphate dodecahydrate, $Na_3PO_4 \cdot 12\ H_2O$, filter sterilised). Seeds were incubated for 20 minutes, keeping them in suspension by inversion. After 20 minutes, TPS was removed with a pipette. Next, seeds were washed with 1 mL of sterile distilled water for 5 consecutive times. Then, 2 mL of commercial bleach (3% sodium hypochlorite) were added to seeds, mixing by inversion again for 20 minutes. Bleach was removed with 1 mL of sterile distilled water, and the washing step repeated for 10 consecutive times. Eventually, sterilized seeds were air-dried on a filter paper inside a flow hood.

IV.7- Plant material and growth conditions

Dry sterilized transgenic seeds were placed in a germination medium (MS salts 4.9 g/L, phytoagar 8.5 g/L, pH = 5.7) supplemented with 100 mg/L kanamycin for positive transgene selection. Control WT plants were obtained similarly by placing seeds in a non-selective germination medium. *In vitro* cultivation of seeds was carried out in a long day growth chamber (16 h light/ 8 h dark, 25ºC, 60–70% humidity, 250 $\mu mol/m^2 \cdot s^1$ photons). A week after germination, WT and kanamycin-resistant seedlings were transferred to the greenhouse, where they were grown in cycles of 16 light hours at 24ºC and 8 dark hours at 20ºC.

On the one hand, WT plants were used in φC31 integrase dose-response assay and in transient expression experiments for characterization of new dCasEV2.1-based memory switches. On the other hand, stably transformed *N. benthamiana* plants with GB1643 (*PB Luc*:*YFP*; Register 2 line) or with GB1644 (*PB*

YFP:*Luc*; Register 4 line) constructs were only used in ϕC31 recombinase dose-response switch activation (SET operation) experiment.

IV.8- Agroinfiltration experiments

Transient expression experiments were performed to test the optimal conditions (promoter and *A. tumefaciens* OD_{600}) for φC31 integrase expression and subsequent switch SET recombination operation (dose-response assay) and to characterize new dCasEV2.1-based memory switches.

For φC31 integrase dose-response assay, *Agrobacterium* cultures with an OD_{600} of 0.2 were prepared. Equal volumes of cultures carrying the different integrase constructs (*P35S:PhiC31R:T35S*, *PNos:PhiC31R:TNos*, *PNtA1:PhiC31R:T35S* and *PNtA11:PhiC31R:T35S*) or constitutive luciferase expression constructs (*PNos:Luc:TNos* and *P35S:Luc:TNos*) and P19 silencing suppressor (GB1203) were mixed so that each culture OD_{600} was 0.1. To obtain 0.01 and 0.001 ODs, 1:10 dilutions were prepared from 0.1 culture mix. Resulting mixes were agroinfiltrated in Register transgenic lines (R2 and R4) and in WT plants.

For transient characterization of new switches, equal volumes of *A. tumefaciens* cultures were mixed so that the final OD_{600} was 0.1. In case a mix didn´t contain the P19 construct, a culture with the P19 vector was added. To balance the total number of *Agrobacterium* cultures in each mixture, a bacterial culture containing a Stuffer Fragment (SF, an empty vector containing a tomato intragenic region) was used (GB0040). In this characterization assays, cell mixes were agroinfiltrated in WT *N. benthamiana* plants.

Agrobacterium individual cultures were first grown from glycerol stocks for two days until saturation, then 10 µL were sub-cultivated in 5 mL of LB media with the corresponding antibiotic and grown for 16 h. First, cultures were pelleted by centrifugation at 3,500 x g for 15 minutes. Then, cell pellets were resuspended in 15 mL of agroinfiltration buffer (10 mM MES, pH 5.6, 10 mM $MgCl_2$ and 200 µM acetosyringone) and incubated in a platform shaker at room temperature for 2 hours in darkness, to avoid acetosyringone photolysis and activate bacterial virulence genes. Once the incubation was finished, OD was measured at 600 nm.

In all transient expression experiments, five-week-old WT or transgenic *N. benthamiana* plants cultivated in the greenhouse (See IV.7- Plant material and growth conditions) were used. Agroinfiltration was carried out using a 1 mL

needleless syringe with which abaxial surface of leaves was infiltrated. In all cases, three leaves per plant were agroinfiltrated, which represent three independent biological replicates per agroinfiltration experiment. Leaf samples were collected 5 days post-infiltration (dpi).

For luciferase expression analysis (bioluminiscence assays), the agroinfiltrated area of each leaf was sampled using a Ø 0.8 cm corkborer (equivalent to 20 mg of tissue). For RNA extractions and downstream qRT-PCR analysis, three discs per agroinfiltrated leaf (approx. 100 mg) were collected. For GC-MS and confocal laser microscopy, a Ø 1.5-2 cm corkborer was used to excise leaf discs. All tissue samples were placed in 2 mL locking lid tubes with metallic beads and immediately frozen in liquid nitrogen. Then, samples were stored at -80ºC until use.

IV.9- Quantification of gene expression

IV.9.1- Luciferase/Renilla reporter assays

Activities of Firefly (Fluc) and Renilla (Rluc) luciferases were determined using the Dual-Glo® Luciferase Assay System (Promega) manufacturer's protocol with minor modifications. Leaf samples were collected 5 dpi in 2 mL locking lid tubes containing a previously added metallic bead, for the homogenization step. One disc with a 0.8 cm diameter was taken per infiltrated leaf (three discs per plant) and immediately frozen in liquid nitrogen. After sampling, tubes were stored at −80ºC for subsequent analysis.

Luc/Ren assays started with the homogenization of frozen samples, which were ground with a Retsch Mixer Mill MM400 for 1 min at 30 Hz. Then, homogenized tissue was mixed with 180 µL of 'Passive Lysis Buffer 1x', vortexed, and centrifuged for 10 min at 13 000 x g and 4ºC. 10 µL from the crude plant extracts (supernatant) were transferred to a 96-well plate and once all samples were loaded, 40 µL of LUCII (Luciferase substrate) was added to each well for Luciferase activity determination.

After Luciferase quantification, 40 µL of Stop&Glow reagent, previously mixed with Renilla substrate 1x, were added to each sample for Renilla activity determination. Measurements were made using a GloMax 96 Microplate Luminometer (Promega) with a 2-s delay and a 10-s measurement for both Luciferase and Renilla activity. Fluc/Rluc ratios were determined as the mean value of three biological replicates, coming from three independent agroinfiltrated leaves of the same plant. These ratio values were normalized to the FLuc/RLuc ratio

obtained for a parallel-assayed WT plant, agroinfiltrated with GB1116 (a construct containing the PNos promoter driving FLuc expression and a 35S promoter driving RLuc expression).

IV.9.2- RNA extraction

At 5 dpi, around 100 mg of agroinfiltrated tissue per leaf was collected in 2 mL locking lid tubes with two metallic beads, and immediately transferred to liquid nitrogen for later storage at −80ºC. RNA extraction started with the grinding of frozen samples on the tissue homogenizer Retsch Mixer Mill MM400 for 30 s at 30 Hz and continued with downstream purification steps using Thermo Scientific's GeneJET Plant RNA Purification Mini Kit, following the manufacturer's protocol. This kit is based on a silica-based membrane column technology which allows a rapid and efficient purification of high-quality total RNA, and higher yields than conventional RNA purification methods.

To avoid RNA degradation, all working surfaces and laboratory material were cleaned with 1% SDS and new RNA-free tips and tubes were used in each RNA extraction round.

IV.9.3- DNA removal from RNA samples

Removal of any DNA contamination (genomic DNA or T-DNA) from RNA samples was an essential step for downstream uses in qRT-PCR gene expression analysis, as during qRT-PCR it is not possible to distinguish genomic DNA/T-DNA from newly synthesized complementary DNA (cDNA). To eliminate DNA, Thermo Fisher Scientific's TURBO DNA-free Kit was utilized. 2 µg of total RNA were mixed with 1 µL of TURBO DNase, 2 µL of its buffer solution 10x TURBO DNase Buffer and nuclease-free water up to 20 µL. Mixture was incubated 30 min at 37ºC. Afterwards, TURBO DNase was inactivated with 2 µL of DNase Inactivation Reagent for 2 min at room temperature. Finally, this mix was centrifuged for 2 additional minutes at 10.000 x g and the supernatant was transferred to new RNA-free tubes. Treated RNA was quantified using Thermo Scientific's NanoDrop 2000c Spectrophotometer.

IV.9.4- cDNA synthesis

RNA samples were reverse transcribed to cDNA following Takara's PrimeScript 1st strand cDNA Synthesis Kit protocol, with minor modifications. cDNA

synthesis was carried out in a 20 µL-thermocycler reaction in two steps: denaturation and reverse transcription. In the denaturation step, 800 µg of DNase-treated RNA were mixed with 0.5 µL dT Primer (50µM) and 0.5 dNTP mix (10 mM each). The reaction was incubated at 65ºC for 5 min and immediately cooled down at 4ºC. Then, in the reverse transcription step, samples were transferred to ice and the following reagents were added: 4 µL of 5x PrimeScript Buffer, 0.25 µL of RNase Inhibitor (40 U/µl), 0.25 µL of PrimeScript RTase (200 U/µL) and free-RNase distilled H_2O up to 20 µL. The mixture was incubated at 42ºC for 30-60 min followed by inactivation at 70ºC for 15 min. cDNA samples were stored at -20 ºC until the qRT-PCR experiments.

IV.9.5- qRT-PCR analysis

Quantitative Real-Time PCRs (qRT-PCRs) were performed to analyse φC31 integrase*, dCas9-EDLL, Luc and YFP* gene transcription levels. Takara's TB Green Premix Ex Taq Master Mix was used (Table 6). In all cases, the *N. benthamiana F-box* gene was selected as an internal reference to measure the relative mRNA expression of each gene. *F-box* gene was amplified using NbFbox_Fw and NbFbox_Rv primers (Supplementary Table 1). From initial cDNA samples, 1:3 or 1:4 working dilutions were prepared and 2 µL were used for qRT-PCR reactions, so that approximately 20 ng of cDNA were analysed per well. Three technical replicates were performed per each biological replicate and measurements were done using Applied Biosystems 7500 Fast Real-Time PCR System. Gene expression data was processed using the system's software QuantStudio Design & Analysis v1.5.1 and the relative expression was calculated using the ΔΔCt method (Livak & Schmittgen, 2001). For analysis of φC31 integrase gene expression, PhiC31R_Fw and PhiC31R_Rv primers were used. In case of *YFP* and *dCas9-EDLL* genes, primers YFP_Fw and YFP_Rv and primers dCas9-EDLL_Fw and dCas9-EDLL_Rv were utilized, respectively. All primer sequences are shown in Supplementary Table 1.

Table 6.- qRT-PCR mix per reaction

Reagent	Volume (µL)
Takara's TB Green Premix Ex Taq Master Mix	10
H_2O	7
Forward oligo (Fw) 5 µM	0,4
Reverse oligo (Rv) 5 µM	0,4
cDNA	2

qRT-PCR primers were designed using the online IDT's PrimerQuest Tool and their efficiency was checked by analysing their performance when amplifying three serial dilutions (1:10, 1:100, 1:1000) from each cDNA sample. Two water negative controls were also amplified to check for primer dimerization.

IV.10- YFP visualization in confocal laser microscopy

Leaf discs (Ø 1.5-2 cm) of either transgenic *N. benthamiana* plants (R4 line, *PB YFP:Luc*), agroinfiltrated with integrase constructs, or of WT *N. benthamiana* plants infiltrated with the *PB dCas9-EDLL:YFP* switch construct were examined 5 dpi under a ZEISS 780 AxioObserver Z1 confocal laser microscope equipped with C Apo 40x/ 1.2 W lens (water immersion) to visualize the yellow fluorescent protein YFP (λ_{ex} = 514 nm; λ_{em} = 517-563 nm). Images of 16 tiles were taken to visualize a larger area and processed with the ZEN 2.6 blue and FIJI software. Brightness and contrast of the unswitched negative controls (P19) and their corresponding switched samples (φC31 integrase-added) in dose-response experiments were equally adjusted to ensure their comparability. In case of *PB dCas9-EDLL*:*YFP* switch characterization experiments brightness and contrast were also equally adjusted. Adjustments made for different switches and/or transitions were not necessarily the same; therefore, comparisons of fluorescence intensity are only valid for each transition.

IV.11- GC-MS moth sex pheromone analysis

50 mg of frozen, ground leaf samples were weighed in a 10 mL headspace screw-cap vial and stabilized by adding 1 mL of 5 M $CaCl_2$ and 150 µL of 500 mM EDTA (pH 7.5), after which they were bath-sonicated for 5 minutes. Volatile compounds were captured by means of headspace solid phase microextraction (HS-

SPME) with a 65 µm polydimethylsiloxane/divinylbenzene (PDMS/DVB) SPME fiber (Supelco, Bellefonte, PA, USA). Volatile extraction was performed automatically by means of a CombiPAL autosampler (CTC Analytics). Vials were first incubated at 80°C for 3 minutes with 500 rpm agitation. The fiber was then exposed to the headspace of the vial for 20 min under the same conditions of temperature and agitation. Desorption was performed at 250°C for 1 minute (splitless mode) in the injection port of a 6890 N gas chromatograph (Agilent Technologies). After desorption, the fiber was cleaned in a SPME fiber conditioning station (CTC Analytics) at 250°C for 5 min under a helium flow. Chromatography was performed on a DB5ms (60 m, 0.25 mm, 1 µm) capillary column (J&W) with helium as the carrier gas at a constant flow of 1.2 mL/min. Oven conditions included an initial temperature of 160°C for 2 min, a 7°C/min ramp until 280°C, and a final hold at 280°C for 6 minutes. Identification of (*Z*)-11-hexadecenol (Z11-16OH) and (*Z*)-11-hexadecenyl acetate (Z11-16OAc) was performed by the comparison of both retention time and mass spectrum with pure standards. Pheromone abundance is expressed as peak area measured in arbitrary units (a.u.).

V.- RESULTS AND DISCUSSION

V.1.- Dose-dependent activation of gene expression by φC31 recombinase

Before this work, Bernabé-Orts et al. (2020) designed the first reversible memory switch for whole plant systems, whose activation was controlled by the bacteriophage φC31 serine integrase (SET operation) and its cognate recombination factor RDF (RESET operation). To characterise this genetic device, several parameters were studied (such as its kinetics, its genetic memory, and its reversibility) in *N. benthamiana* plants through transient and stable transformation experiments. However, the optimal dose-dependent activation of the switch by the φC31 recombinase remained to be determined. As reported by Vazquez-Vilar et al. (2017b), high φC31 integrase doses had a repressive effect on a luciferase reporter construct containing an *attR* site. For this reason, setting the optimal integrase dose was essential for a proper control of switch activation. In this work, we have focused on optimizing the switch SET operation, where the switch *PB* configuration turns to the *RL* state when the φC31 integrase is supplied. Dose-response assays were carried out by transient expression, agroinfiltrating φC31 recombinase in two *N. benthamiana* transgenic lines in which the switch is stably integrated: Register 2 line (R2), carrying the switch construct *PB Luc*:*YFP* (GB1643), where the *YFP* gene is switched on (ON) and the *Luc* gene remains transcriptionally inactive (OFF); and Register 4 line (R4) carrying the *PB YFP*:*Luc* construct (GB1644) where, on the contrary, the *Luc* gene is ON and the *YFP* gene is OFF (Figure 3).

To determine the optimal conditions for the switch SET operation, two parameters were studied, which affect the quantity of φC31 integrase available to bind to and recombine the *att* sites in the switch:

1. The influence of promoter strength driving φC31 integrase expression and subsequent switch activation, generating four φC31 constructs driven by promoters of different strengths: the CaMV 35S promoter (P35S) (GB1497), the Nopaline synthase promoter (PNos) (GB1531) and the *Nicotiana tabacum* promoters, PNtA11 (GB4021) and PNtA1 (GB022). Promoter strength range from the strongest to the weakest promoter was: P35S > PNos > PNtA1 > PNtA11. Assuming a value of 1 for PNos promoter strength, expected promoter strengths equal 10 for P35S, 1.17 for PNtA1 and 0.08 for PNtA11.
2. The influence of *A. tumefaciens* optical density (OD_{600}), assaying three different ODs: 0.1, 0.01 and 0.001.

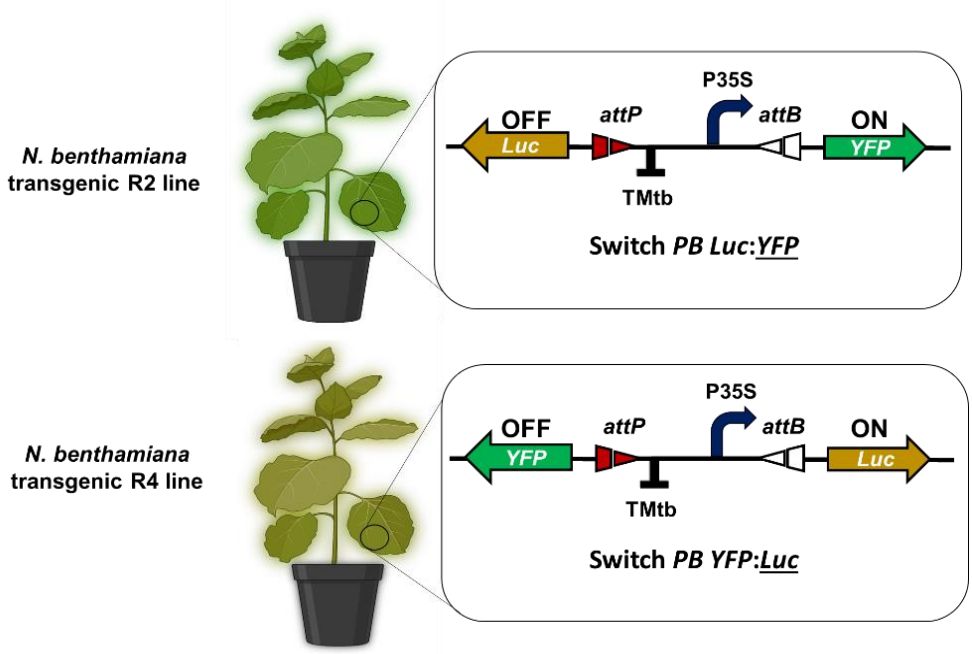

Figure 3.- Description of *N. benthamiana* R2 and R4 transgenic lines. Plants from line R2 carry the switch construct in *PB* configuration *Luc*:*YFP* (GB1643), where the *YFP* gene is transcriptionally active (ON) and the *Luc* gene remains inactive (OFF), whereas plants from line R4 carry the *YFP*:*Luc* switch construct in *PB* state (GB1644), where *Luc* gene is ON and *YFP* gene is OFF. Both transgenic lines were generated by Bernabé-Orts et al. (2020).

Taking into consideration both parameters, a total of 12 conditions were assayed through transient expression of φC31 integrase in R2 and R4 lines. Twelve R2 plants and twelve R4 plants, and three leaves per plant, were agroinfiltrated as depicted in Figure 4. For each condition, each leaf represents an independent biological replicate. At the same time, three WT *N. benthamiana* plants (three whole leaves per plant) were infiltrated with control constructs: *PNos:Luc:TNos* (GB1116) and *P35S:Luc:TNos* (GB0164) for the constitutive expression of the *Luc* gene, and the negative control carrying only the P19 suppressor of silencing. At 5 dpi, leaf disc samples from the agroinoculated area were excised. Samples were then processed according to their genotype: samples from line R4 were used to visualize switch-controlled YFP activation under the confocal microscope, while samples from line R2 were used in bioluminiscence assays to measure switch-controlled luciferase expression (Figure 4).

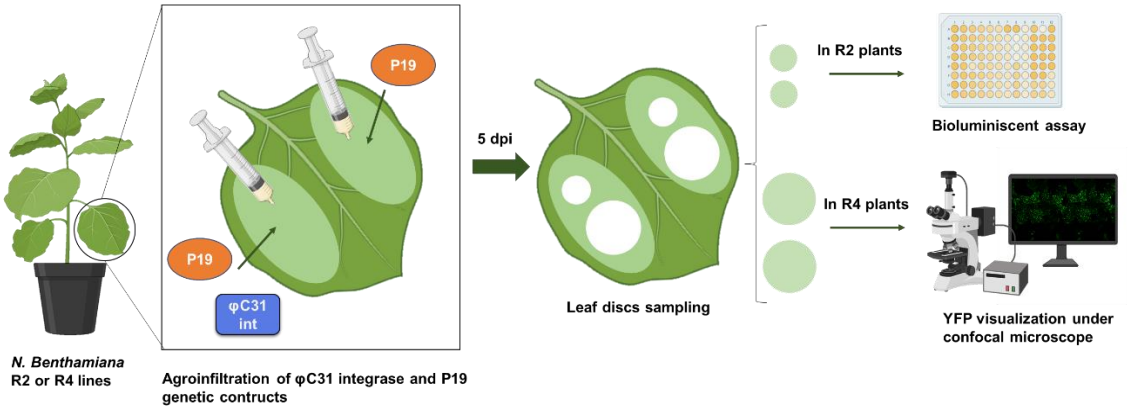

Figure 4.- Dose-response experiments workflow. Three leaves of each Register plant, either from the R2 or R4 line, were agroinfiltrated as shown in the picture. The left side of leaves was infiltrated with an *Agrobacterium* mix, at the appropriate OD_{600}, containing the corresponding φC31 integrase construct (φC31 int), depicted as a blue rectangle, and P19 silencing suppressor construct (P19), represented as an orange oval. The right side was infiltrated solely with P19 at the same OD_{600} used on the left, representing a negative control of switch-mediated gene activation for each leaf. 5 dpi, two small leaf discs (one per half leaf) were collected in R2 plants, which were later used in bioluminescence assays to measure switch-mediated luciferase expression. In R4 lines, two large discs were sampled and subsequently visualized under the confocal microscope to see switch-controlled YFP activation.

The visualization of YFP levels under the confocal microscope in R4 leaf discs revealed that in all infiltration conditions the YFP protein was expressed after φC31 integrase supply, and its cellular localization was spread throughout the nuclei and cytoplasm. As it was expected, the lowest *Agrobacterium* OD_{600} (0.001) coupled to any of the four promoters for the expression of the integrase resulted in low levels of YFP activation, since only a few cells were fluorescent, as shown in Figure 5B. For the intermediate OD_{600} 0.01, all promoters gave higher YFP activation than for OD_{600} 0.001, as it can be observed in confocal images, where a higher number of cells are expressing the fluorescent protein. This result was expected, since the higher the *Agrobacterium* OD_{600}, the greater the number of integrase copies which can enter *N. benthamiana* cells, and the more *PB YFP:Luc* switches can be turned to the *RL YFP:Luc* state (Figure 5A), giving higher YFP expression. Nevertheless, in general, infiltration of the φC31 integrase at the highest OD 0.1 did not result in a proportional increase of YFP activation, as the number of fluorescent cells was comparable to the one obtained with the intermediate OD_{600} 0.01. In the case of the low-strength PNtA11 promoter, confocal microscopy showed an apparent increase of YFP intensity and of the number of switched-on cells. Surprisingly, when the strongest promoter P35S was used together with the maximum OD_{600} 0.1, switch-mediated

YFP activation was very low with a small number of fluorescent cells, resembling YFP levels achieved with the lowest OD_{600} 0.001 (Figure 5B).

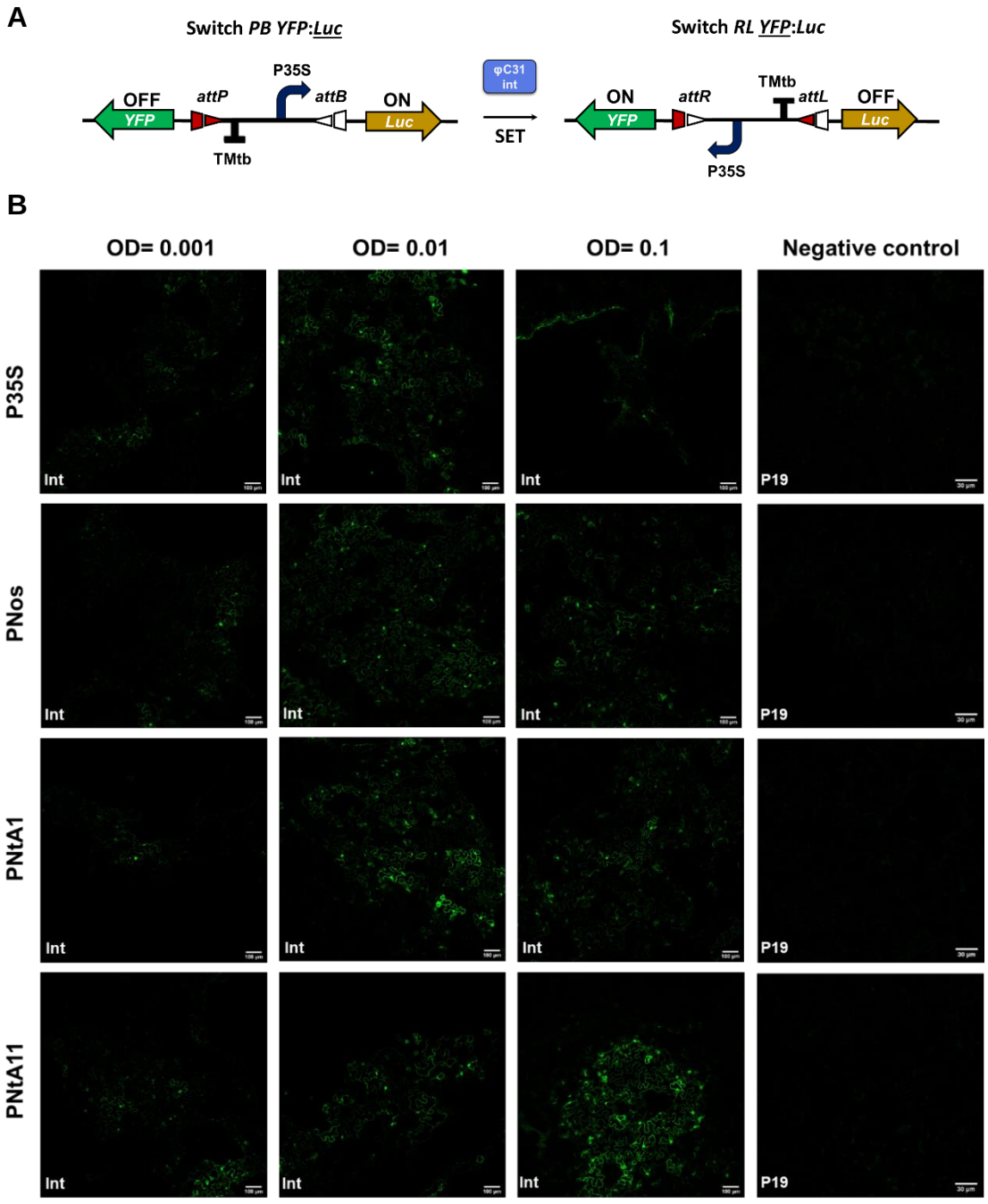

Figure 5.- YFP visualization in stable *N. benthamiana* R4 plants (*PB YFP:Luc*) after φC31 integrase addition (*RL YFP:Luc*). (A) SET operation in switch *PB Luc:YFP*. After φC31 recombinase addition, *Luc* gene turns inactive (OFF) and *YFP* gene is activated (ON), allowing its visualization under the confocal microscope. (B) Confocal laser microscopy images, taken 5 dpi, of R4 *N. benthamiana* transgenic leaves agroinfiltrated with φC31 integrase (Int) constructs driven by different promoters: P35S (GB1497), PNos (GB1531), PNtA1 (GB4022) and PNtA11 (GB4021); at three OD_{600nm}: 0.001, 0.01 and 0.1. All infiltrations included a construct carrying the silencing suppressor P19. Negative controls were infiltrated with P19 alone.

After qualitative measurements of YFP, leaf disc samples from R2 plants supplied with φC31 recombinase were processed for their use in bioluminescent assays which aimed to quantitatively measure luciferase activity, coming from the activation of the *Luc* gene in switch *PB Luc*:*YFP* after the addition of the phage recombinase (*RL Luc:YFP* state) (Figure 6A). Agroinfiltration of all the constructs expressing the φC31 recombinase with different promoters at OD_{600} 0.001 resulted in similar luciferase activation levels, with FLuc/RLuc values between 2.5 and 4.2, with no significant differences between promoters (Figure 6B). This result confirmed the poor YFP levels previously reported in R4 leaf discs when infiltrating the recombinase using such a low OD_{600}. Normalized luciferase activities when using the intermediate OD_{600} 0.01 or the highest 0.1 and any of the four promoters, independently of their strength, resulted in non-significant activation levels between both OD_{600} values, suggesting a saturation kinetics of the φC31 integrase-controlled switch device. Thus, at *Agrobacterium* OD_{600} higher than 0.01, the switch is probably saturated and completely turned to the *RL* state, with no further increase on gene activation.

Except for the P35S promoter, infiltrations with PNos, PNtA1 and PNtA11 promoters at the intermediate OD_{600} 0.01 induced higher luciferase activations than luciferase levels obtained at OD_{600} 0.001. Interestingly, FLuc/RLuc values achieved with the strongest promoter (P35S) at the three *Agrobacterium* OD_{600} were similar, with no statistical differences among the lowest, the intermediate or the highest OD_{600}. In addition, the use of the P35S promoter and the maximum OD_{600} 0.1 resulted in much lower luciferase activity than expected, with a normalized luciferase mean value (FLuc/RLuc) of 6.5 against 22.8, 32.8 and 24.95 for the PNos, PNtA1 and PNtA11 promoters at the same OD_{600}, respectively. This low luciferase activity paralleled the low YFP levels seen in R4 leaves infiltrated in the same conditions (Figure 5B).

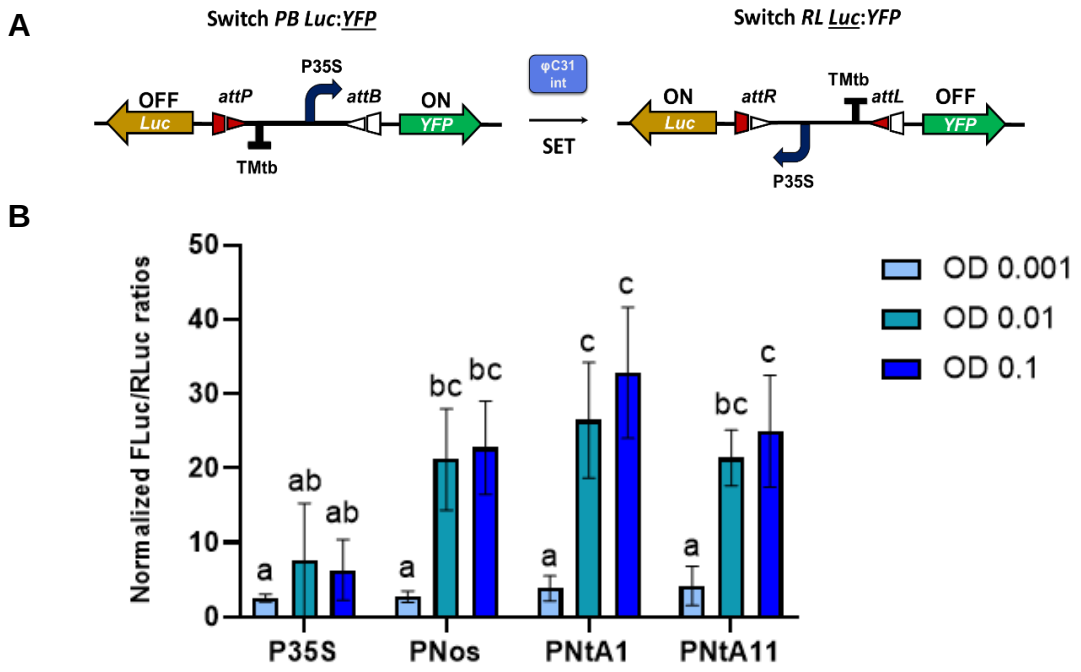

Figure 6.- **Luciferase activation in *N. benthamiana* R2 plants (*PB Luc:YFP*) after φC31 integrase supply.** (A) Schema of SET operation in switch *PB Luc:YFP*. After the addition of φC31 recombinase, *YFP* gene turns transcriptionally inactive (OFF) and *Luc* gene is activated (ON) (state *RL Luc:YFP*), enabling its quantitative measurement through a bioluminescent assay. (B) Quantification of luciferase activity in leaves of *N. benthamiana* R2 transgenic plants infiltrated with four φC31 integrase constructs where recombinase is driven by different promoters: P35S (GB1497), PNos (GB1531), PNtA1 (GB4022) and PNtA11 (GB4021); at three optical densities (OD): 0.001, 0.01 and 0.1. Bars represent the mean of normalized Fluc/Rluc values of three agroinfiltrated leaves (n=3) ± SD. Statistical analysis was performed using Two-way ANOVA (Tukey's multiple comparisons test, P-Value ≤ 0.05). Bars with the same letter (a, b or c) are non-significant (ns) and bars with different letters are statistically significant.

V.2.- High doses of φC31 integrase have a repressive activity on gene expression

Since higher doses of φC31 recombinase (supplied with either higher-strength promoters or higher *Agrobacterium* concentrations) did not result linearly in higher levels of *GOI* activation, but instead suggested a saturation curve, we decided to further elucidate the activation dynamic by quantifying φC31 recombinase transcripts in the different experimental conditions.

Three leaves of transgenic R2 plants (*PB Luc*:*YFP*) were agroinfiltrated with the integrase (thus turning to *RL Luc*:*YFP*) as explained before (Figure 4), but this time the four promoter constructs controlling integrase expression were assayed at only one OD_{600}, 0.1. After 5 days, two small leaf discs (one per half leaf) from agroinfiltrated areas were taken for subsequent luciferase activity measurements. In addition, three leaf discs (approx. 100 mg) from the left side of R2 leaves, infiltrated

with the φC31 recombinase, were collected for later RNA isolation and qRT-PCR analysis.

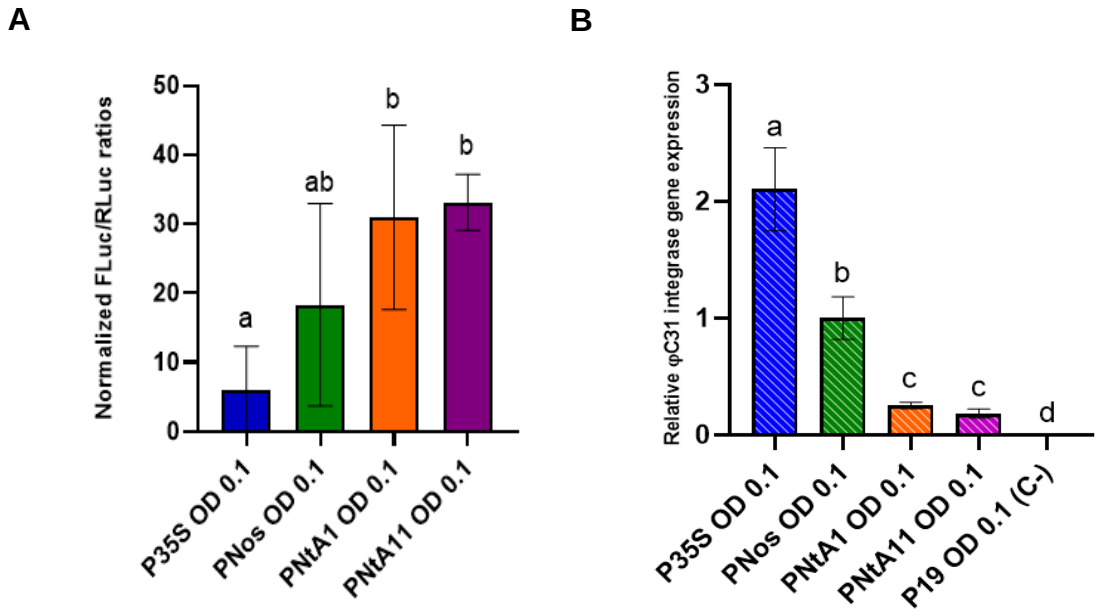

Figure 7.- Repressive activity of the φC31 integrase over *PB Luc*:*YFP* switch. (A) Quantification of luciferase activity in leaves of *N. benthamiana* R2 transgenic plants after inoculation with *Agrobacterium* cultures at OD 0.1 containing four φC31 integrase constructs driven by different strength promoters: P35S, PNos, PNtA1 and PNtA11. (B) qRT-PCR analysis of φC31 integrase gene expression under the control of different promoters. Represented expression values are relative to the gene expression levels of φC31 integrase gene driven by PNos promoter. Bars represent the mean of normalized FLuc/Rluc or relative integrase gene expression values of three agroinfiltrated leaves (n=3) ± SD. Statistical analyses were performed using unpaired t-test, P-Value ≤ 0.05.

At OD_{600} 0.1, all constructs displayed similar luciferase activation levels to the ones obtained in the previous bioluminescence assay (Figure 6B), confirming that lower promoter strengths (like PNtA1 or PNtA11) yielded higher luciferase switch-mediated activation than the stronger promoters (such as P35S). The lower luciferase activation using the P35S promoter for integrase expression was not dependent on a transcriptional issue, since φC31 integrase gene expression levels were high, as expected for such a strong promoter as P35S (Figure 7B). Moreover, as it can be seen comparing both graphs (Figures 7A and 7B), there is a tendency in which the higher the expression of integrase gene, the lower the luciferase activation in the switch. Luciferase data, together with transcriptional analysis, show that the φC31 integrase has an *Agrobacterium* OD_{600}-dependent repressive activity over the memory switch. These results confirm the repressive effect of φC31 recombinase reported by Vazquez-Vilar et al. (2017b) in a luciferase reporter

construct driven by 35S promoter that contained an *attR* site, when the integrase was added at high levels. One possible explanation for the repressive activity of φC31 integrase could be that when the integrase is present at high levels, it maintains its ability to bind to *att* sites but it does not catalyse site-specific recombination. The binding of many integrases might eventually prevent transcription of *GOIs* in the switch by steric hindrance, consequently decreasing switch-controlled gene activation.

After analysing and comparing data from switch-mediated YFP activation levels and luciferase activity assays in all tested conditions and taking into consideration the transcriptional analysis of the φC31 recombinase gene, we decided to choose promoter PNtA1 and *Agrobacterium* OD_{600} 0.01 as optimal conditions for φC31 integrase-mediated switch SET operation**.** PNos and PNtA11 at OD_{600} 0.01 displayed similar luciferase activation levels (Figure 6B). We chose PNtA1 because we reasoned that this promoter would ensure intermediate levels of φC31 integrase, sufficient to guarantee activation in all circumstances and low enough to avoid transcriptional repression.

V.3.- Design and characterization of new dCasEV2.1-based switches

Once the optimal conditions for φC31 recombinase expression and subsequent switch SET operation were identified, two new dCasEV2.1-based switches were designed and functionally characterized by transient expression in *N. benthamiana* WT plants. These new versions combined the switch genetic device with the dCasEV2.1 gene activation system (Selma et al., 2019). Combining both synthetic tools would allow to regulate not only the expression of genes controlled by the switch, but also the activation of several genes through the dCasEV2.1 system using promoter-specific gRNAs.

Two new switches were designed and assembled through GB cloning in pDGB3 Ω1 destination vectors together with the transcriptional activator fusion MS2:VPR, necessary for the assembly of the dCasEV2.1 activation complex, and the hygromycin plant resistance gene (*HygroR*) for prospective stable integration in plants. The first design was the *PB dCas9-EDLL*:*YFP* switch (Figure 8A), and the second was the *PB dCas9-EDLL*:*Luc* switch (Figure 8B), in which the *YFP* and *Luc* genes remain active (ON) until the intentional addition of the φC31 integrase, respectively. The two kinds of design allowed us to conduct different kinds of assays (fluorescence- or bioluminescence-based) to characterize the activity of the switch.

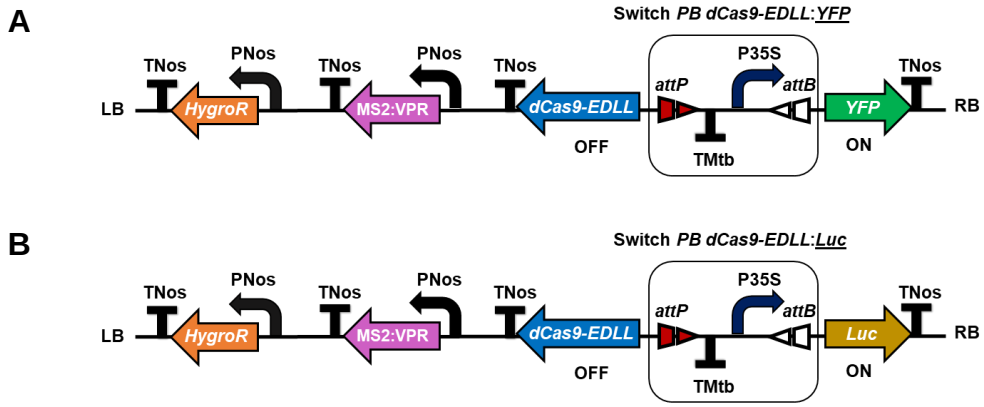

Figure 8.- Representation of dCasEV2.1-based switch DNA constructs. These constructs carry the hygromycin plant resistance gene (*HygroR*), the transcriptional activator fusion MS2:VPR necessary for the assembly of dCasEV2.1 gene activation complex and *PB dCas9-EDLL*:*YFP* switch (GB4147) (A) or *PB dCas9-EDLL*:*Luc* switch (GB4145) (B).

Three whole leaves of *N. benthamiana* WT plants were agroinfiltrated with *Agrobacterium* culture mixes, where each culture contained a different DNA construct. Total OD_{600} of each mix was 0.1 and the individual OD_{600} for each culture was 0.02, with the exception of the PNtA1:φC31 integrase construct, which was infiltrated at 0.01, since this was the optimal optical density for switch SET activation, as concluded before.

First, we wanted to test the ability of the *dCas9-EDLL*:*YFP* switch to regulate the activation of a downstream luciferase reporter construct (called S.P.7.4:Luc; GB3331) driven by a synthetic *S. lycopersicum DFR*-based promoter. To do so, the genetic construct containing *dCas9-EDLL*:*YFP* and the MS2:VPR transcriptional activator (GB4147) was co-infiltrated with the PNtA1-controlled φC31 integrase construct, the luciferase reporter S.P.7.4:Luc and a guide RNA complementary to the DFR promoter (gDFR; GB2515). The combinations of agroinfiltrated constructs are shown in Figure 9B, where the presence/absence of a DNA construct in each *Agrobacterium* mix is represented with +/-, respectively. Our first hypothesis was the following: once all DNA constructs were expressed in a plant cell, the integrase would switch on the expression of the *dCas9-EDLL* gene (*RL dCas9-EDLL*:*YFP*). The dCas9-EDLL fusion protein would bind the gDFR guide, which would also allow the recruitment of the MS2-VPR chimeric transcriptional activators, thanks to the MS2 anchoring sites on the scaffold sequence. This strong transcriptional activation complex, called dCasEV2.1, would specifically target the *DFR*-based synthetic promoter of the S.P.7.4:Luc reporter, eventually activating luciferase expression (Figure 9A). The initial hypothesis was accepted, since as it can be seen in Figure

9B (second green bar), that after φC31 integrase addition, the S.P.7.4 luciferase reporter was activated with a FLuc value of 5.03 times the constitutive control PNos:Luc (FLuc = 1). The downstream luciferase activation by dCasEV2.1 complex gave a similar FLuc value to the direct measurement of luciferase in switch *PB dCas9-EDLL*:*Luc*, where luciferase is constantly being expressed (Figure 9B, first blue bar). We were also able to conclude that the dCasEV2.1 activation system regulated by the memory switch is gRNA-specific, since when a non-specific gRNA was used (gPNos; GB1724) S.P.7.4:Luc activation was significantly reduced to a normalized FLuc value (relative to PNos:Luc) of 0.01. The great drawback we identified in this experiment regarding the *PB dCas9-EDLL*:*YFP* switch is its leakiness, since in the absence of φC31 integrase the luciferase reporter was equally activating at comparable levels. FLuc activation without the integrase was not significantly different to the luciferase activation after integrase addition (Figure 9B, green bars).

This leakiness was also observed when we aimed to regulate a pheromone biosynthetic pathway in *N. benthamiana* WT plants. This pathway was previously expressed in transgenic *N. benthamiana* plants by Mateos-Fernández et al. (2021). In this work, the *EaDAct* acetyltransferase gene used by Mateos-Fernández et al. (2021) was substituted by the *ScATF1* acetyltransferase gene from *S. cerevisiae*, since the latter encodes a more efficient enzyme (Ding et al., 2016). In this case, we co-infiltrated the following constructs:

1. a construct carrying the *PB dCas9-EDLL*:*Luc* switch and the MS2:VPR and *HygroR* TUs (see Figure 8B)
2. a construct carrying the integrase, regulated by the PNtA1 promoter
3. a construct carrying a pheromone biosynthetic pathway, in which each gene (*AtrΔ11*, *HarFAR* and *ScATF1*) is controlled by a synthetic *DFR*-based promoter, together with the constitutively expressed gDFR guide RNA (GB3897)

As before, the integrase would allow the assembly of the dCasEV2.1 complex and, in this case, the production of the volatile Lepidopteran sex pheromones (Figure 10A). Analysis of GC-MS chromatograms revealed that, when no integrase was added, both (*Z*)-11-hexadecenol and (*Z*)-11-hexadecenyl acetate mean compound peak areas (a.u.) were 1,10E+07 and 3,87E+06, respectively. When the integrase was supplied, (*Z*)-11-hexadecenol and (*Z*)-11-hexadecenyl acetate peak values were 7,68E+06 and 3,56E+06 a.u., respectively (Figure 10B). Differences between

pheromone production values were not statistically significant, revealing high leakiness levels, which confirm the tendency observed by measuring the expression of the S.P.7.4:Luc reporter.

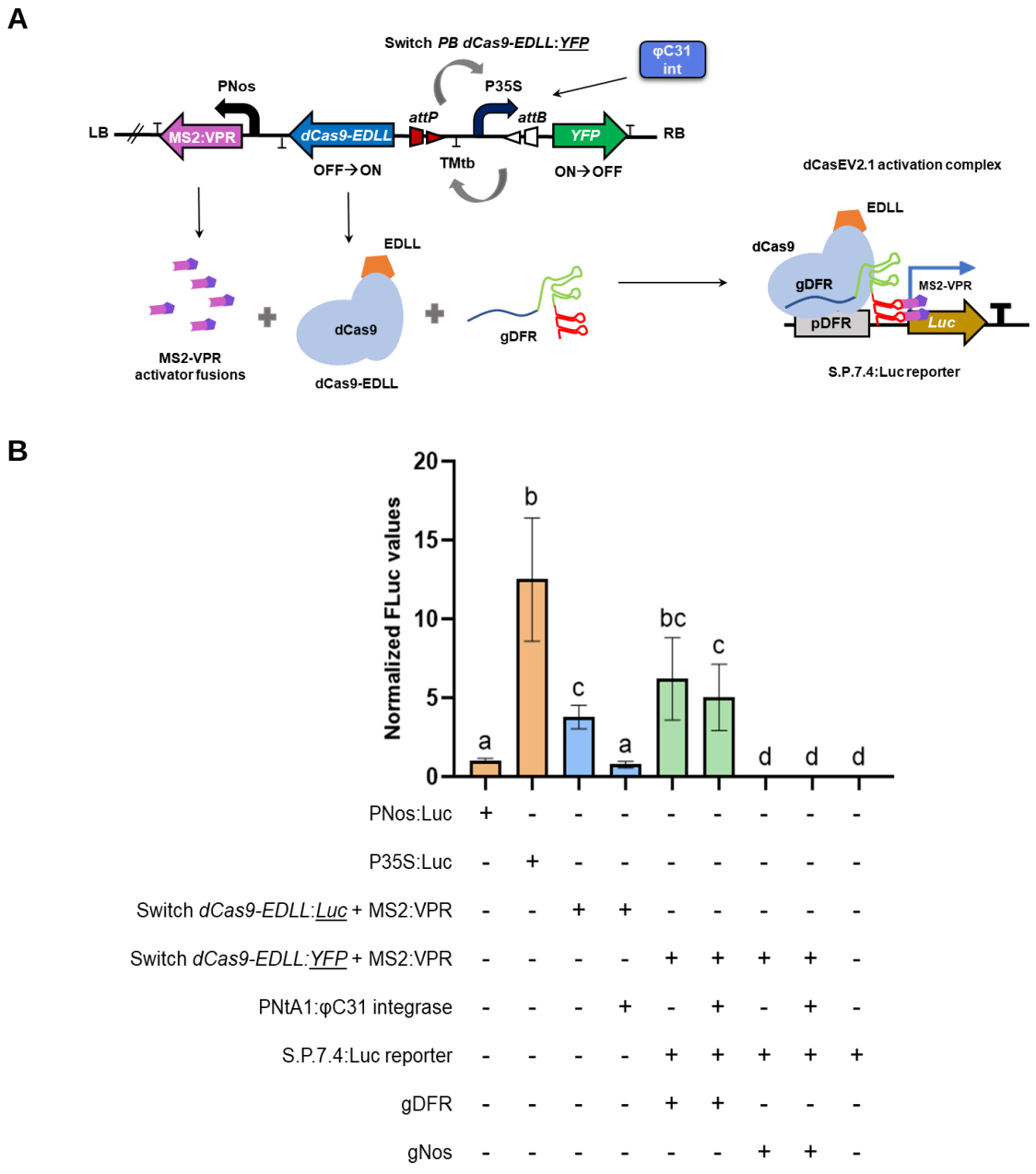

Figure 9.- **Luciferase activation through dCasEV2.1-based switches.** (A) Representation of downstream luciferase reporter activation regulated by memory switch *PB dCas9-EDLL:YFP* switch. After φC31 integrase addition, dCasEV2.1 complex can be assembled and targeted to S.P.7.4 luciferase reporter, through a gDFR RNA guide, giving rise to luciferase activity. (B) Luciferase activation through dCasEV2.1-based switches at 5 dpi. Bars represent the mean of normalized FLuc values of three agroinfiltrated leaves (n=3) ± SD. Statistical analyses were performed using unpaired t-test, P-Value ≤ 0.05. The presence/absence of a DNA construct in each *Agrobacterium* culture mix is represented with +/-, respectively.

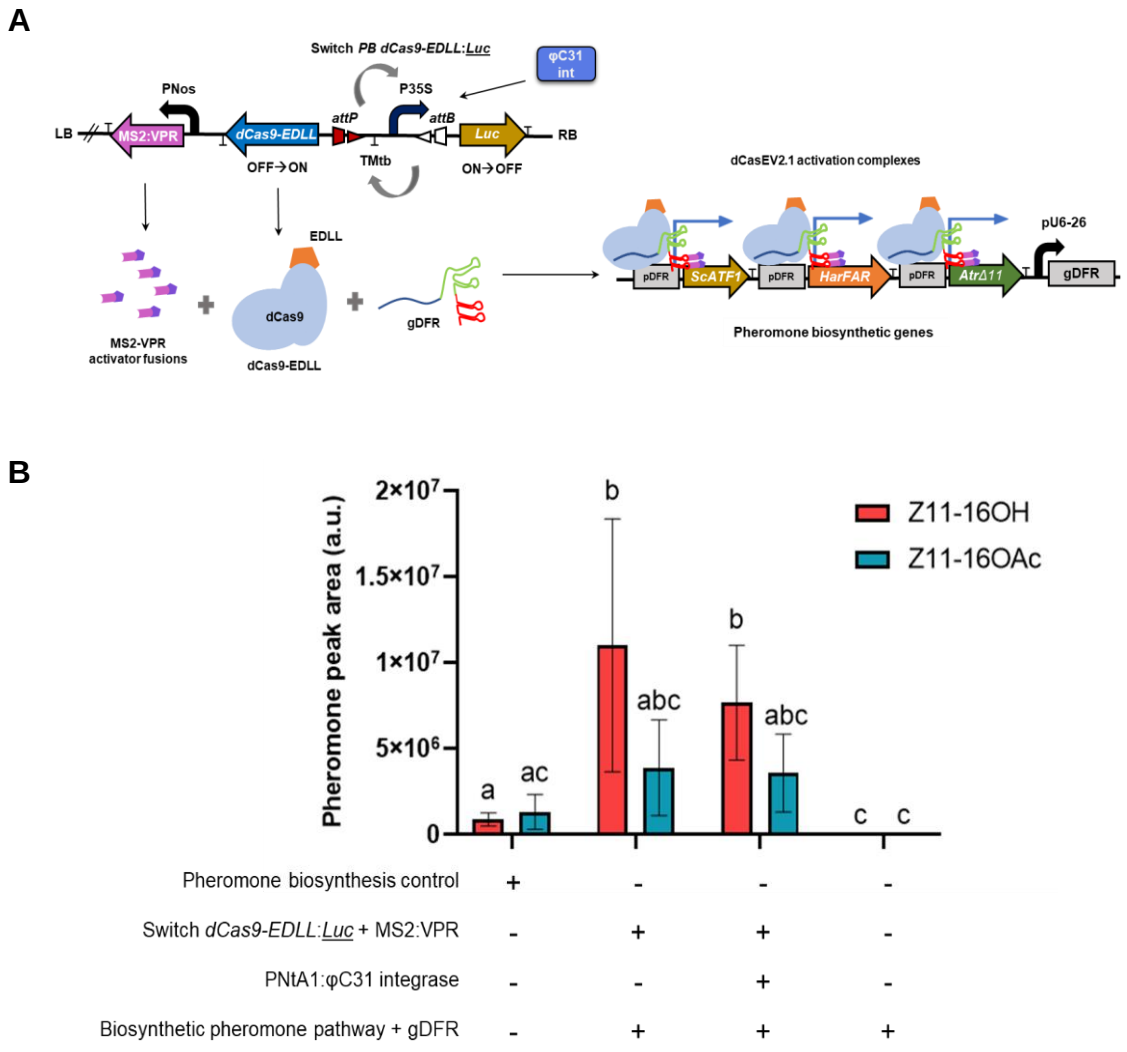

Figure 10.- **Lepidopteran sex pheromone production through dCasEV2.1-based switch *PB dCas9-EDLL:Luc*.** (A) Schematic representation of dCasEV2.1-mediated pheromone biosynthetic pathway activation and regulated by memory switch *PB dCas9-EDLL:Luc* switch. After φC31 integrase addition, dCasEV2.1 complex can be assembled and gDFR-mediated targeted to pheromone biosynthesis genes (*ATF1, HarFAR* and *AtrΔ11*) driven by DFR promoters (pDFR), giving rise to volatile pheromone production. (B) Lepidoptera pheromone production in agroinfiltrated *N. benthamiana* leaves at 5 dpi. Bars represent the mean peak areas in arbitrary units (a.u.) of two volatile moth sex pheromones, (*Z*)-11-hexadecenol (Z11-16OH) or (*Z*)-11-hexadecenyl acetate (Z11-16OAc), produced in three agroinfiltrated leaves (n=3) ± SD. The pheromone biosynthesis control comprised the *ATF1, HarFAR* and *AtrΔ11* genes constitutively expressed (GB4407). Statistical analyses were performed using One-way ANOVA (Tukey's multiple comparisons test, P-Value ≤ 0.05).

We hypothesized that both dCasEV2.1-based switches were leaky due to the influence of other promoters present in the construct adjacent to the switch (Figure 8), such as the PNos promoter driving the expression of MS2:VPR, which could be affecting *dCas9-EDLL* expression in the switch independently of φC31 integrase supply. This hypothesis was tested by comparing the effect of delivering the

PNos:MS2:VPR:TNos TU on the same T-DNA as the switch (in *cis*), or delivering it on a different construct (GB2511) mixed with the *PB dCas9-EDLL:YFP* switch (*i.e.*, in *trans*), when agroinfiltrating WT *N. benthamiana* plants. In both cases, the constructs carrying the gDFR guide, the S.P.7.4:Luc reporter and the PNtA1:φC31 integrase were co-infiltrated with the switch and the *PNos:MS2:VPR:TNos* TU. Luciferase activation assay showed that the delivery of MS2:VPR in *trans* determined, despite not significant, a small reduction in the leakiness of the switch device (Supplementary Figure 2). Therefore, in the following experiments MS2:VPR was infiltrated in the *trans* configuration.

Finally, to deeply understand switch leakiness at transcriptional level, we analysed by qRT-PCR the expression of the genes controlled by switch *PB dCas9-EDLL*:*YFP*, *dCas9-EDLL* and *YFP*, before and after the addition of the φC31 integrase. We also visualized YFP levels under the confocal microscope, to compare *YFP* transcript levels and fluorescence of *N. benthamiana* cells carrying *PB dCas9-EDLL*:*YFP*. In addition, we measured bioluminescence levels of a downstream luciferase reporter as described before, obtaining the same luciferase activation trend shown in Supplementary Figure 2 (data not shown). For this purpose, three whole leaves of *N. benthamina* WT plants were agroinfiltrated with:

1. a switch construct carrying *dCas9-EDLL*:*YFP* (GB4146)
2. the MS2:VPR transcriptional activator in *trans* (GB4147)
3. the φC31 integrase construct
4. the luciferase reporter S.P.7.4:Luc
5. the gDFR guide RNA

After 5 days, disc leaf samples from each agroinfiltrated leaf were collected for subsequent RNA isolation and qRT-PCR analysis, YFP visualization under the confocal microscope and bioluminescence assays.

As shown in Figure 11A, YFP levels in cells agroinfiltrated with the switch construct *PB dCas9-EDLL*:*YFP* were very high, as it was expected for this switch configuration, where YFP is ON. When the switch was co-infiltrated with the φC31 integrase construct, many fluorescent cells switched off, as can be clearly observed in the right image of Figure 11A. Gene expression analysis by quantitative RT-PCR revealed that when the integrase was infiltrated together with the memory switch construct, *dCas9-EDLL* and *YFP* transcript levels fluctuated as expected. After the addition of the φC31 recombinase, *dCas9-EDLL* expression had a 1.84-fold increase while *YFP* expression had a 1.64-fold decrease with respect to their expression levels in switch

configuration before integrase supply (Figure 11B). *YFP* expression levels after integrase addition bore out the fluorescence decrease observed in *N. benthamiana* cells. Both gene expression increase and decrease were not statistically significant, demonstrating that the switch was also leaky at the transcriptional level. In addition to the lack of significance, the relative fold change was not big enough to cause a major shift in dCas9-EDLL protein activity between the two states. On the other hand, the decrease of YFP fluorescence (Figure 11A) and the differences in transcript levels between *YFP* and *dCas9-EDLL* after recombinase addition (Figure 11B) indicate that the φC31 integrase can flip the switch from the *PB* state to the *RL* configuration.

A

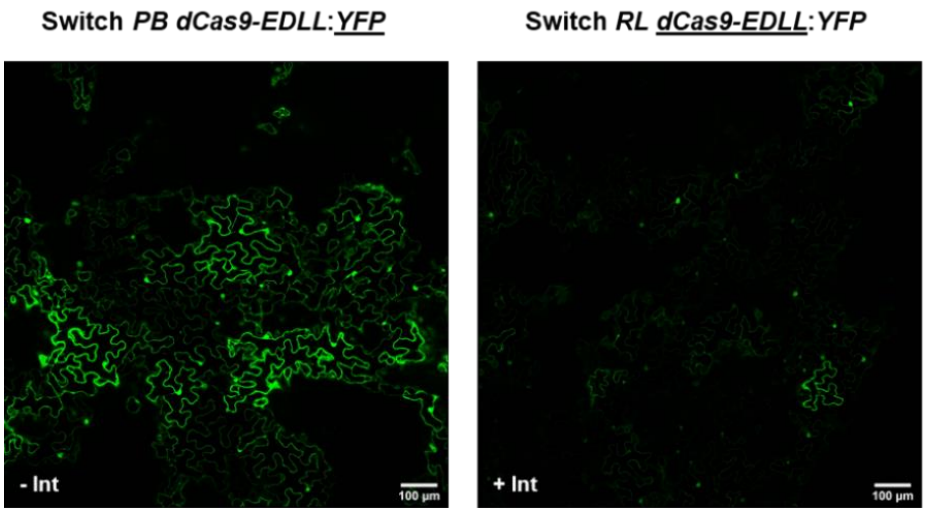

B

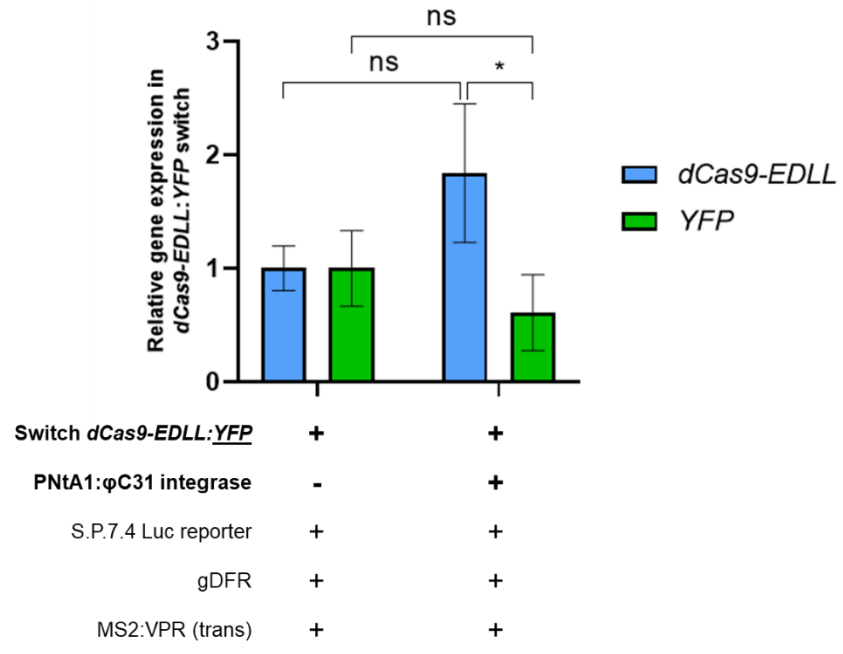

Figure 11.- **Functional characterization by transient expression of memory switch *PB dCas9-EDLL:YFP* in *N. benthamina* WT plants.** (A) Confocal laser microscopy images taken 5 dpi of WT *N. benthamiana* leaves agroinfiltrated with *PB dCas9-EDLL:YFP* construct without or with the co-infiltration of PNtA1:φC31 phage integrase (- Int or + Int, respectively). It can be observed that after integrase addition, YFP fluorescence in cells is decreased. (B) Analysis of gene expression by qRT-PCR of genes controlled by switch. Bars represent the mean of normalized relative *YFP* or *dCas9-EDLL* gene expression values of three agroinfiltrated leaves (n=3) ± SD. Shown expression values are relative to the expression levels of *YFP* and *dCas9-EDLL* genes in *PB dCas9-EDLL:YFP* switch configuration, when no integrase is added. Statistical analysis were performed using unpaired t-test, *P-Value ≤ 0.05.

All data together indicate that new switch versions, which combine the dCasEV2.1 activation system (Selma et al., 2019) with the φC31 integrase-based memory switch (Bernabé-Orts et al., 2020), are not capable of precisely regulating the expression of downstream target genes (either luciferase or the pheromone biosynthetic pathway), since these genes are expressed also in the absence of the integrase. This is a great drawback from a regulatory perspective, since the main interest in switch genetic tools lies in their ability to tightly regulate the expression of a gene of interest. For this reason, the combination of these two regulatory synthetic tools must be further understood and more precisely tuned. In this study, the MS2:VPR chimeric activator was expressed constitutively. High levels of MS2:VPR, together with the constitutive expression of the guide RNAs, could favor the undesired activation of the dCas9-EDLL protein regulated by the new switch versions even in the absence of the integrase. In the future, one possible solution to avoid switch leakiness could be to double regulate through different switches the expression of the MS2:VPR chimeric activator and of the *dCas9-EDLL* gene. Another solution to decrease leakiness could be to redesign the switch central core by using alternative promoters, which could interact differently with the adjacent CDSs and yield tighter regulation. The use of lower strength promoters, such as PNos, PNtA1 or PNtA11, could improve the regulatory function of the switch, as the current use of strong promoter such as P35S could be affecting *dCas9-EDLL* expression even when the gene is switched off.

VI.- CONCLUSIONS

From the results obtained in this Master thesis we can conclude that:

- High doses of φC31 integrase have a repressive activity over gene expression in genes regulated by the memory switch.
- The optimal phage φC31 integrase dose for switch-mediated gene activation (SET operation) is achieved when the integrase is expressed under the *N. tabacum* promoter PNtA1 at the *A. tumefaciens* C58 OD_{600} 0.01.
- When the *Agrobacterium* OD_{600} is higher than 0.01, the switch is saturated with no further increase in gene activation.
- The two new switches based on the dCasEV2.1 activation system, *PB dCas9-EDLL*:*YFP* and *PB dCas9-EDLL*:*Luc*, are functional in transient expression in *N. benthamiana* plants, and can activate downstream target genes with the appropriate guide RNAs.
- The new switch synthetic biotools are unable to ensure tight regulation of the downstream pathways and need to be redesigned to precisely control the activation of target genes of interest in plants, inducing activation only when the φC31 integrase is supplied.

VII.- BIBLIOGRAPHY

Andres, J., Blomeier, T., & Zurbriggen, M. D. (2019). Synthetic switches and regulatory circuits in plants. *Plant Physiology*, *179*(3), 862–884. https://doi.org/10.1104/pp.18.01362

Aoyama, T., & Chua, N.-H. (1997). A glucocorticoid-mediated transcriptional induction system in transgenic plants. In *The Plant Journal* (Vol. 11, Issue 3).

Baltes, N. J., & Voytas, D. F. (2015). Enabling plant synthetic biology through genome engineering. In *Trends in Biotechnology* (Vol. 33, Issue 2, pp. 120–131). Elsevier Ltd. https://doi.org/10.1016/j.tibtech.2014.11.008

Barrangou, R., Fremaux, C., Deveau, H., Richards, M., Boyaval, P., Moineau, S., Romero, D. A., & Horvath, P. (2007). CRISPR Provides Acquired Resistance Against Viruses in Prokaryotes. *Science*, *315*(5819), 1709–1712. https://doi.org/10.1126/science.1138140

Bernabé-Orts, J. M., Quijano-Rubio, A., Vazquez-Vilar, M., Mancheño-Bonillo, J., Moles-Casas, V., Selma, S., Gianoglio, S., Granell, A., & Orzaez, D. (2020). A memory switch for plant synthetic biology based on the phage ϕc31 integration system. *Nucleic Acids Research*, *48*(6), 3379–3394. https://doi.org/10.1093/nar/gkaa104

Böhmdorfer, G., Tramontano, A., Luxa, K., & Bachmair, A. (2010). A synthetic biology approach allows inducible retrotransposition in whole plants. *Systems and Synthetic Biology*, *4*(2), 133–138. https://doi.org/10.1007/s11693-010-9053-4

Caddick, M. X., Greenland, A. J., Jepson, lan, Krause, K.-P., Qu, N., Riddell, K. v., Salter, M. G., Schuch, W., Sonnewald, U., & Tomsett, A. B. (1998). An ethanol inducible gene switch for plants used to manipulate carbon metabolism. *Nature Biotechnology*, *16*(2), 177–180. https://doi.org/10.1038/nbt0298-177

Cameron, D. E., Bashor, C. J., & Collins, J. J. (2014). A brief history of synthetic biology. In *Nature Reviews Microbiology* (Vol. 12, Issue 5, pp. 381–390). Nature Publishing Group. https://doi.org/10.1038/nrmicro3239

Chatelle, C., Ochoa-Fernandez, R., Engesser, R., Schneider, N., Beyer, H. M., Jones, A. R., Timmer, J., Zurbriggen, M. D., & Weber, W. (2018). A Green-Light-Responsive System for the Control of Transgene Expression in Mammalian and Plant Cells. *ACS Synthetic Biology*, *7*(5), 1349–1358. https://doi.org/10.1021/acssynbio.7b00450

Chavez, A., Scheiman, J., Vora, S., Pruitt, B. W., Tuttle, M., P R Iyer, E., Lin, S., Kiani, S., Guzman, C. D., Wiegand, D. J., Ter-Ovanesyan, D., Braff, J. L., Davidsohn, N., Housden, B. E., Perrimon, N., Weiss, R., Aach, J., Collins, J. J., & Church, G. M. (2015). Highly efficient Cas9-mediated transcriptional programming. *Nature Methods*, *12*(4), 326–328. https://doi.org/10.1038/nmeth.3312

Deltcheva, E., Chylinski, K., Sharma, C. M., Gonzales, K., Chao, Y., Pirzada, Z. A., Eckert, M. R., Vogel, J., & Charpentier, E. (2011). CRISPR RNA maturation by trans-encoded small RNA and host factor RNase III. *Nature*, *471*(7340), 602–607. https://doi.org/10.1038/nature09886

Ding, B. J., Lager, I., Bansal, S., Durrett, T. P., Stymne, S., & Löfstedt, C. (2016). The Yeast ATF1 Acetyltransferase Efficiently Acetylates Insect Pheromone Alcohols: Implications for the

Biological Production of Moth Pheromones. *Lipids*, *51*(4), 469–475. https://doi.org/10.1007/s11745-016-4122-4

Diretto, G., Al-Babili, S., Tavazza, R., Papacchioli, V., Beyer, P., & Giuliano, G. (2007). Metabolic Engineering of Potato Carotenoid Content through Tuber-Specific Overexpression of a Bacterial Mini-Pathway. *PLoS ONE*, *2*(4), e350. https://doi.org/10.1371/journal.pone.0000350

Elowitz, M. B., & Leibler, S. (2000). A synthetic oscillatory network of transcriptional regulators. *Nature*, *403*(6767), 335–338. https://doi.org/10.1038/35002125

Engler, C., Kandzia, R., & Marillonnet, S. (2008). A one pot, one step, precision cloning method with high throughput capability. *PLoS ONE*, *3*(11). https://doi.org/10.1371/journal.pone.0003647

Feng, Z., Zhang, Z., Hua, K., Gao, X., Mao, Y., Botella, J. R., & Zhu, J. K. (2018). A highly efficient cell division-specific CRISPR/Cas9 system generates homozygous mutants for multiple genes in arabidopsis. *International Journal of Molecular Sciences*, *19*(12). https://doi.org/10.3390/ijms19123925

Gardner, T. S., Cantor, C. R., & Collins, J. J. (2000). Construction of a genetic toggle switch in Escherichia coli. In *NATURE* (Vol. 403). www.nature.com

Garner, K. L. (2021). Principles of synthetic biology. In *Essays in Biochemistry* (Vol. 65, Issue 5, pp. 791–811). Portland Press Ltd. https://doi.org/10.1042/EBC20200059

Grindley, N. D. F., Whiteson, K. L., & Rice, P. A. (2006). Mechanisms of Site-Specific Recombination. *Annual Review of Biochemistry*, *75*(1), 567–605. https://doi.org/10.1146/annurev.biochem.73.011303.073908

Jansing, J., Sack, M., Augustine, S. M., Fischer, R., & Bortesi, L. (2019). CRISPR/Cas9-mediated knockout of six glycosyltransferase genes in Nicotiana benthamiana for the production of recombinant proteins lacking β-1,2-xylose and core α-1,3-fucose. *Plant Biotechnology Journal*, *17*(2), 350–361. https://doi.org/10.1111/pbi.12981

Jiang, W., Bikard, D., Cox, D., Zhang, F., & Marraffini, L. A. (2013). RNA-guided editing of bacterial genomes using CRISPR-Cas systems. *Nature Biotechnology*, *31*(3), 233–239. https://doi.org/10.1038/nbt.2508

Jinek, M., Chylinski, K., Fonfara, I., Hauer, M., Doudna, J. A., & Charpentier, E. (2012). A programmable dual-RNA-guided DNA endonuclease in adaptive bacterial immunity. *Science*, *337*(6096), 816–821. https://doi.org/10.1126/science.1225829

Khaleel, T., Younger, E., Mcewan, A. R., Varghese, A. S., & Smith, M. C. M. (2011). A phage protein that binds ϕC31 integrase to switch its directionality. *Molecular Microbiology*, *80*(6), 1450–1463. https://doi.org/10.1111/j.1365-2958.2011.07696.x

Konermann, S., Brigham, M. D., Trevino, A. E., Joung, J., Abudayyeh, O. O., Barcena, C., Hsu, P. D., Habib, N., Gootenberg, J. S., Nishimasu, H., Nureki, O., & Zhang, F. (2015). Genome-scale transcriptional activation by an engineered CRISPR-Cas9 complex. *Nature*, *517*(7536), 583–588. https://doi.org/10.1038/nature14136

Kristensen, C., Morant, M., Olsen, C. E., Ekstrøm, C. T., Galbraith, D. W., Lindberg Møller, B., & Bak, S. (2005). Metabolic engineering of dhurrin in transgenic Arabidopsis plants with

marginal inadvertent effects on the metabolome and transcriptome PLANT BIOLOGY. In *PNAS February* (Vol. 1, Issue 5). www.pnas.orgcgidoi10.1073pnas.0409233102

Li, Z., Zhang, D., Xiong, X., Yan, B., Xie, W., Sheen, J., & Li, J. F. (2017). A potent Cas9-derived gene activator for plant and mammalian cells. *Nature Plants*, *3*(12), 930–936. https://doi.org/10.1038/s41477-017-0046-0

Liu, W., & Stewart, C. N. (2015). Plant synthetic biology. In *Trends in Plant Science* (Vol. 20, Issue 5, pp. 309–317). Elsevier Ltd. https://doi.org/10.1016/j.tplants.2015.02.004

Livak, K. J., & Schmittgen, T. D. (2001). Analysis of Relative Gene Expression Data Using Real-Time Quantitative PCR and the 2−ΔΔCT Method. *Methods*, *25*(4), 402–408. https://doi.org/10.1006/meth.2001.1262

Lowder, L. G., Zhang, D., Baltes, N. J., Paul, J. W., Tang, X., Zheng, X., Voytas, D. F., Hsieh, T. F., Zhang, Y., & Qi, Y. (2015). A CRISPR/Cas9 toolbox for multiplexed plant genome editing and transcriptional regulation. *Plant Physiology*, *169*(2), 971–985. https://doi.org/10.1104/pp.15.00636

Maioli, A., Gianoglio, S., Moglia, A., Acquadro, A., Valentino, D., Milani, A. M., Prohens, J., Orzaez, D., Granell, A., Lanteri, S., & Comino, C. (2020). Simultaneous CRISPR/Cas9 Editing of Three PPO Genes Reduces Fruit Flesh Browning in Solanum melongena L. *Frontiers in Plant Science*, *11*. https://doi.org/10.3389/fpls.2020.607161

Mateos-Fernández, R., Moreno-Giménez, E., Gianoglio, S., Quijano-Rubio, A., Gavaldá-García, J., Estellés, L., Rubert, A., Rambla, J. L., Vazquez-Vilar, M., Huet, E., Fernández-del-Carmen, A., Espinosa-Ruiz, A., Juteršek, M., Vacas, S., Navarro, I., Navarro-Llopis, V., Primo, J., & Orzáez, D. (2021). Production of Volatile Moth Sex Pheromones in Transgenic Nicotiana benthamiana Plants. *BioDesign Research*, *2021*, 1–17. https://doi.org/10.34133/2021/9891082

McCarty, N. S., Graham, A. E., Studená, L., & Ledesma-Amaro, R. (2020). Multiplexed CRISPR technologies for gene editing and transcriptional regulation. In *Nature Communications* (Vol. 11, Issue 1). Nature Research. https://doi.org/10.1038/s41467-020-15053-x

Mett, V., Farrance, C. E., Green, B. J., & Yusibov, V. (2008). Plants as biofactories. In *Biologicals* (Vol. 36, Issue 6, pp. 354–358). https://doi.org/10.1016/j.biologicals.2008.09.001

Mojica, F. J. M., Díez-Villaseñor, C., García-Martínez, J., & Soria, E. (2005). Intervening sequences of regularly spaced prokaryotic repeats derive from foreign genetic elements. *Journal of Molecular Evolution*, *60*(2), 174–182. https://doi.org/10.1007/s00239-004-0046-3

Müller, K., Siegel, D., Rodriguez Jahnke, F., Gerrer, K., Wend, S., Decker, E. L., Reski, R., Weber, W., & Zurbriggen, M. D. (2014). A red light-controlled synthetic gene expression switch for plant systems. *Molecular BioSystems*, *10*(7), 1679–1688. https://doi.org/10.1039/c3mb70579j

Nielsen, A. Z., Ziersen, B., Jensen, K., Lassen, L. M., Olsen, C. E., Møller, B. L., & Jensen, P. E. (2013). Redirecting photosynthetic reducing power toward bioactive natural product synthesis. *ACS Synthetic Biology*, *2*(6), 308–315. https://doi.org/10.1021/sb300128r

Oldroyd, G. E. D., & Dixon, R. (2014). Biotechnological solutions to the nitrogen problem. In *Current Opinion in Biotechnology* (Vol. 26, pp. 19–24). https://doi.org/10.1016/j.copbio.2013.08.006

Pan, C., Sretenovic, S., & Qi, Y. (2021). CRISPR/dCas-mediated transcriptional and epigenetic regulation in plants. In *Current Opinion in Plant Biology* (Vol. 60). Elsevier Ltd. https://doi.org/10.1016/j.pbi.2020.101980

Papikian, A., Liu, W., Gallego-Bartolomé, J., & Jacobsen, S. E. (2019). Site-specific manipulation of Arabidopsis loci using CRISPR-Cas9 SunTag systems. *Nature Communications*, *10*(1). https://doi.org/10.1038/s41467-019-08736-7

Park, S.-H., Zarrinpar, A., & Lim, W. A. (2003). Rewiring MAP Kinase Pathways Using Alternative Scaffold Assembly Mechanisms. *Science*, *299*(5609), 1061–1064. https://doi.org/10.1126/science.1076979

Piatek, A., Ali, Z., Baazim, H., Li, L., Abulfaraj, A., Al-Shareef, S., Aouida, M., & Mahfouz, M. M. (2015). RNA-guided transcriptional regulation in planta via synthetic dCas9-based transcription factors. *Plant Biotechnology Journal*, *13*(4), 578–589. https://doi.org/10.1111/pbi.12284

Qi, L. S., Larson, M. H., Gilbert, L. A., Doudna, J. A., Weissman, J. S., Arkin, A. P., & Lim, W. A. (2013). Repurposing CRISPR as an RNA-Guided Platform for Sequence-Specific Control of Gene Expression. *Cell*, *152*(5), 1173–1183. https://doi.org/10.1016/j.cell.2013.02.022

Roberts, G. R., Garoosi, G. A., Koroleva, O., Ito, M., Laufs, P., Leader, D. J., Caddick, M. X., Doonan, J. H., & Tomsett, A. B. (2005). The alc-GR system. A modified alc gene switch designed for use in plant tissue culture. *Plant Physiology*, *138*(3), 1259–1267. https://doi.org/10.1104/pp.105.059659

Saijo, T., & Nagasawa, A. (2014). Development of a tightly regulated and highly responsive copper-inducible gene expression system and its application to control of flowering time. *Plant Cell Reports*, *33*(1), 47–59. https://doi.org/10.1007/s00299-013-1511-5

Sánchez-León, S., Gil-Humanes, J., Ozuna, C. v., Giménez, M. J., Sousa, C., Voytas, D. F., & Barro, F. (2018). Low-gluten, nontransgenic wheat engineered with CRISPR/Cas9. *Plant Biotechnology Journal*, *16*(4), 902–910. https://doi.org/10.1111/pbi.12837

Sarrion-Perdigones, A., Falconi, E. E., Zandalinas, S. I., Juárez, P., Fernández-del-Carmen, A., Granell, A., & Orzaez, D. (2011). GoldenBraid: An iterative cloning system for standardized assembly of reusable genetic modules. *PLoS ONE*, *6*(7). https://doi.org/10.1371/journal.pone.0021622

Sarrion-Perdigones, A., Palaci, J., Granell, A., & Orzaez, D. (2014). Design and construction of multigenic constructs for Plant biotechnology using the GoldenBraid cloning strategy. *Methods in Molecular Biology*, *1116*, 133–151. https://doi.org/10.1007/978-1-62703-764-8_10

Sarrion-Perdigones, A., Vazquez-Vilar, M., Palací, J., Castelijns, B., Forment, J., Ziarsolo, P., Blanca, J., Granell, A., & Orzaez, D. (2013). Goldenbraid 2.0: A comprehensive DNA assembly framework for plant synthetic biology. *Plant Physiology*, *162*(3), 1618–1631. https://doi.org/10.1104/pp.113.217661

Sedeek, K. E. M., Mahas, A., & Mahfouz, M. (2019a). Plant genome engineering for targeted improvement of crop traits. In *Frontiers in Plant Science* (Vol. 10). Frontiers Media S.A. https://doi.org/10.3389/fpls.2019.00114

Sedeek, K. E. M., Mahas, A., & Mahfouz, M. (2019b). Plant genome engineering for targeted improvement of crop traits. In *Frontiers in Plant Science* (Vol. 10). Frontiers Media S.A. https://doi.org/10.3389/fpls.2019.00114

Selma, S., Bernabé-Orts, J. M., Vazquez-Vilar, M., Diego-Martin, B., Ajenjo, M., Garcia-Carpintero, V., Granell, A., & Orzaez, D. (2019). Strong gene activation in plants with genome-wide specificity using a new orthogonal CRISPR/Cas9-based programmable transcriptional activator. In *Plant Biotechnology Journal* (Vol. 17, Issue 9, pp. 1703–1705). Blackwell Publishing Ltd. https://doi.org/10.1111/pbi.13138

Storozhenko, S., de Brouwer, V., Volckaert, M., Navarrete, O., Blancquaert, D., Zhang, G. F., Lambert, W., & van der Straeten, D. (2007). Folate fortification of rice by metabolic engineering. *Nature Biotechnology*, *25*(11), 1277–1279. https://doi.org/10.1038/nbt1351

Vazquez-Vilar, M., Quijano-Rubio, A., Fernandez-Del-Carmen, A., Sarrion-Perdigones, A., Ochoa-Fernandez, R., Ziarsolo, P., Blanca, J., Granell, A., & Orzaez, D. (2017a). GB3.0: a platform for plant bio-design that connects functional DNA elements with associated biological data. *Nucleic Acids Research*, *45*(4), 2196–2209. https://doi.org/10.1093/nar/gkw1326

Vazquez-Vilar, M., Quijano-Rubio, A., Fernandez-Del-Carmen, A., Sarrion-Perdigones, A., Ochoa-Fernandez, R., Ziarsolo, P., Blanca, J., Granell, A., & Orzaez, D. (2017b). GB3.0: a platform for plant bio-design that connects functional DNA elements with associated biological data. *Nucleic Acids Research*, *45*(4), 2196–2209. https://doi.org/10.1093/nar/gkw1326

von Caemmerer, S., Quick, W. P., & Furbank, R. T. (2012). The development of C4 rice: Current progress and future challenges. In *Science* (Vol. 336, Issue 6089, pp. 1671–1672). American Association for the Advancement of Science. https://doi.org/10.1126/science.1220177

Way, J. C., Collins, J. J., Keasling, J. D., & Silver, P. A. (2014). Integrating biological redesign: Where synthetic biology came from and where it needs to go. In *Cell* (Vol. 157, Issue 1, pp. 151–161). Elsevier B.V. https://doi.org/10.1016/j.cell.2014.02.039

Weinmann, P., Gossen, M., Hillen, W., Bujard, H., & Getz, C. (1994). A chimeric transactivator allows tetracycline-responsive gene expression in whole plants. In *The Plant Journal* (Vol. 5, Issue 4).

Xie, K., Minkenberg, B., & Yang, Y. (2015). Boosting CRISPR/Cas9 multiplex editing capability with the endogenous tRNA-processing system. *Proceedings of the National Academy of Sciences of the United States of America*, *112*(11), 3570–3575. https://doi.org/10.1073/pnas.1420294112

Yang, T., Deng, L., Zhao, W., Zhang, R., Jiang, H., Ye, Z., Li, C. B., & Li, C. (2019). Rapid breeding of pink-fruited tomato hybrids using the CRISPR/Cas9 system. In *Journal of Genetics and Genomics* (Vol. 46, Issue 10, pp. 505–508). Institute of Genetics and Developmental Biology. https://doi.org/10.1016/j.jgg.2019.10.002

Zalatan, J. G., Lee, M. E., Almeida, R., Gilbert, L. A., Whitehead, E. H., la Russa, M., Tsai, J. C., Weissman, J. S., Dueber, J. E., Qi, L. S., & Lim, W. A. (2015). Engineering complex synthetic

transcriptional programs with CRISPR RNA scaffolds. *Cell*, *160*(1–2), 339–350. https://doi.org/10.1016/j.cell.2014.11.052

VIII.- SUPPLEMENTARY MATERIAL

VIII.1.- Annex I. GB plasmids and Oligonucleotides.

Supplementary Table 1.- GB parts generated and used in this study

GB code	Name	Description
GB1190	pEGB 35S:dCas9-EDLL:tNOS	TU for the expression of the dCas9 with the activation domain EDLL as a CT fusion.
GB1643	TNos:NptII:Pnos-SF PB (LUC:YFP)-35s:Ren:TNos	Module for the stable transformation of the Register PB (*Luc*:*YFP*). Contains a TU for the constitutive expression of Ren.
GB1644	TNos:NptII:Pnos-SF PB (YFP:LUC)-35s:Ren:TNos	Module for the stable transformation of the Register PB (*YFP:Luc*). Contains a TU for the constitutive expression of Ren.
GB1497	pEGB_3alpha1 P35S:PhiC31:T35S	TU for constitutive expression of *Streptomyces* phage phiC31 integrase. Catalyzes site-specific recombination between phiC31 attB and attP sites. Contains SV40 NLS. *N. benthamiana* codon optimized.
GB1531	pEGB_3alpha1 PNos:PhiC31:TNos	TU for constitutive expression of Streptomyces phage phiC31 integrase. Catalyzes site-specific recombination between phiC31 attB and attP sites. Contains SV40 NLS. *N. benthamiana* codon optimized.
GB4021	pDGB3 alpha1 PNtA11:PhiC31 integrase:T35S	TU for constitutive expression of Streptomyces phage PhiC31 integrase driven by *Nicotiana tabacum* NtA11 promoter. PhiC31 integrase catalyzes site-specific recombination between phiC31 *attB* and *attP* sites.
GB4022	pDGB3 alpha1 PNtA1:PhiC31 integrase:T35S	TU for constitutive expression of *Streptomyces* phage PhiC31 integrase driven by *Nicotiana tabacum* NtA1 promoter. PhiC31 integrase catalyzes site-specific recombination between phiC31 *attB* and *attP* sites.
GB3331	Omega1_R:US7.4:miniDFR:luc:t35s +P19(TU) +Renilla(TU)	Module for the regulated expression of Firefly Luciferase driven by the minimal slDFR promoter with a synthetic upstream sequence containing three targets for the gRNA-1DFR, and for the constitutive expression of Renilla and P19.
GB4145	pDGB3_omega1 Tnos:HygroR: Pnos-SF-Tnos:VPR:MS2:Pnos-SF + Register PB dCas9-EDLL:Luc	Bistable element composed of TMtb:P35S, flanked by PhiC31 site- specific recombination sites attP and attB, inverted CDS of dCas9-EDLL and direct Luc CDS. Constitutive expression of Hygromycin plant resistance and MS2:VPR for dCas9-EDLL activation
GB4147	pDGB3_omega1 Tnos:HygroR:Pnos-SF-Tnos:VPR:MS2:Pnos-SF + Register PB dCas9-EDLL:YFP	Bistable element composed of TMtb:P35S, flanked by PhiC31 site- specific recombination sites attP and attB, inverted CDS of dCas9-EDLL and direct YFP CDS. Constitutive expression

		of Hygromycin plant resistance and MS2:VPR for dCas9-EDLL activation.
GB2515	alpha2 gRNA 2.1 SlDFR -150	Cassette for the expression of a guide RNA targeting the *DFR* promoter with two MS2 aptamer copies in the 3' of the scaffold
GB1724	pDGB3_alpha1_U6-26:gRNA (pNos):MS2 F6x2 aptamer	Target for the Nopaline Synthetase Promoter (PNos) with the MS2 recognition loop in position 3' in the scaffold
GB1203	pEGB 35s:P19:tNos	TU for the expression of the silencing suppressor P19 driven by the 35S promoter
GB3897	Alpha2_nptII+SF+INS+ATF1+ HarFar+AtrD11+gRNA1 DFR	Module for the inducible expression of AtrD11, HarFar and ATF1 using dCasEV2.1 system, the *nptII* gene for selection and the gRNA-1DFR (SexyPlant's Guided-pathway).
GB4407	3o2 AtrD11_HarFar_SF_ATF1	pDGB3α2 for the constitutive expression of the *H. armigera* fatty acid reductase, the *A. transitella* delta-11-desaturase and the alcohol O-acetyltransferase from *S. cerevisiae* S288C, codon optimized, with a SF.
GB1116	pEGB PNos:Luciferase:TNos-SF-35S:Renilla:TNos-35S:P19:TNos-SF	Module for the expression of the Firefly Luciferase, the Renilla Luciferase and the P19 silencing suppressor (standard reference in pCambia for luciferase experiments)
GB0164	pEGB 35s:Luciferase:Tnos-SF-35s:Renilla:Tnos-35s:P19:Tnos (Module)	Module for the expression of the Firefly luciferase, the Renilla luciferasa and the P19 silencing supressor genes driven by the 35s promoter and the Nos terminator
GB2511	alpha2:PNos:MS2:VPR:Tnos	TU for expression of MS2 coat protein fused to VPR.
GB4146	Register PhiC31 PB dCas9-EDLL:YFP (Tnos:dCas9-EDLL:attP:TMtb:P35S:attB:YFP:Tnos)	Bistable element composed of TMtb:P35S. Flanked by opposing PhiC31 site-specific recombination sites (attP and attB), inverted CDS of dCas9-EDLL and direct of YFP. Initial state → YFP expression. Addition PhiC31 integrase → dCas9-EDLL expression.
GB0040	pSF	*S. lycopersicum* intergenic region (stuffer fragment)

Supplementary Table 2.- Primers used in this work

Code	Primer sequence (5'→ 3')	Length (nt)	GC %	Tm (ºC)
SGS21ABR01_Fw	GCGCCGTCTCGCTCGGGAGCGAGTCGGTCCCATTATTGA	39	50.00	62.30
SGS21ABR02_Rv	GCGCCGTCTCGCTCAATAGTTCTAGTCGAAATGCCCAAGA	40	42.86	62.30
PhiC31R_Fw	AAGAGCAGACGCCTTGAATGCA	22	50.00	59.21
PhiC31R_Rv	TGCGCCTTGCTGTCTCAAAGTT	22	50.00	59.66
YFP_Fw	CAGAAGAACGGCATCAAGGT	20	50.00	54.60
YFP_Rv	TGGTAGCTCAGGTAGTGGTT	20	50.00	54.00
dCas9-EDLL_Fw	GACGCTAACCTCGATAAGGTGCTT	24	50.00	58.70
dCas9-EDLL_Rv	TGTCGAAGTACTTGAAGGCTGCAG	24	50.00	59.10
NbFbox_Fw	TTGGAAACTCTCTCCCCACTTG	22	50.00	55.98
NbFbox_RV	GCTCATTGTTGGATGGGTACCT	22	50.00	56.45

VIII.2.- Annex II. Supplementary Figures

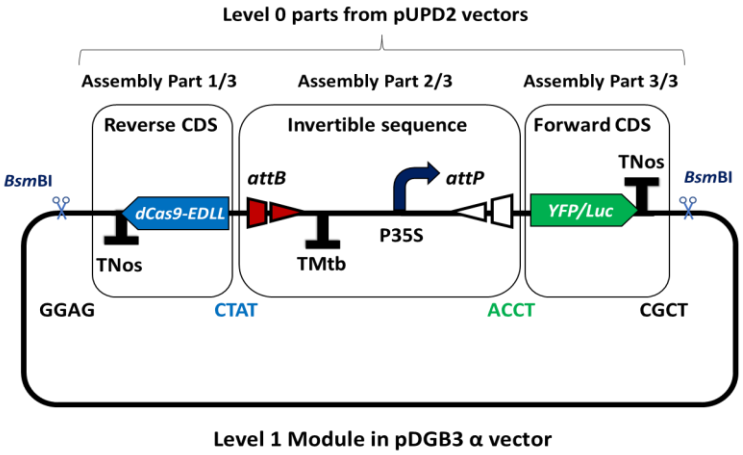

Supplementary Figure 1.- Structure of *PB*-state genetic memory dCasEV2.1-based switches designed and assembled in this Master's thesis. Switches are divided into three basic DNA assembly parts: part 1/3, corresponds to the *dCas9-EDLL* reverse-oriented coding sequence (CDS); part 2/3 corresponds to the core of the switch, formed by a terminator TMtb and a 35S promoter sequence flanked by *attB* and *attP* specific recombination sites; and part 3/3 represent the direct-oriented CDS of *YFP* or *Luc* gene, depending on the switch. The dCas9-EDLL CDS was domesticated *de novo* using the overhangs pictured in this Figure (GGAG and CTAT) for its assembly in a pUPD2 vector (Level 0 assembly part 1/3) and its later cloning in a pDGB3 vector together with the rest of pre-existing assembly parts, creating a DNA switch (Level 1 construct).

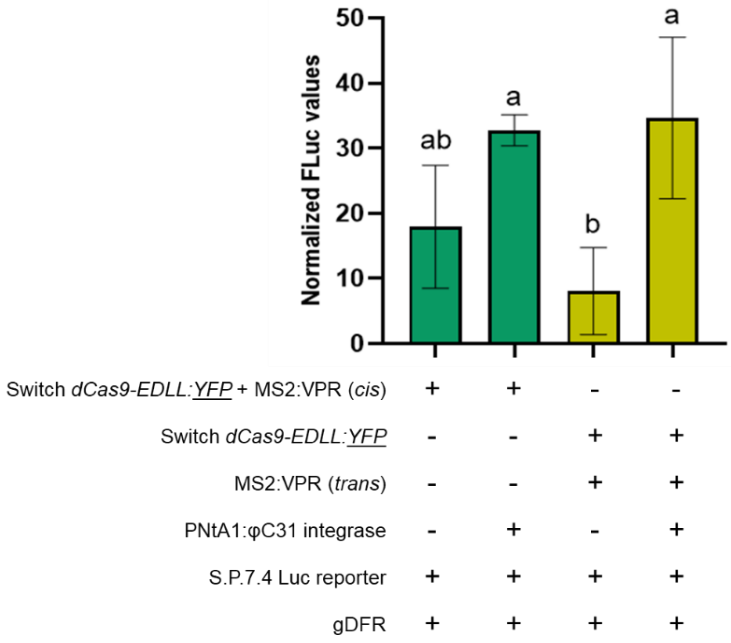

Supplementary Figure 2.- Effect of MS2:VPR construct (GB2511) agroinfiltration in *trans* on switch *dCas9-EDLL:YFP* leakiness. Luciferase activation through dCasEV2.1-based switch at 5 dpi. The infiltration of MS2:VPR in *trans* (first light green bar) reduced, despite not significantly, switch leakiness observed when MS2:VPR was agroinfiltrated in *cis* configuration (first dark green bar). Bars represent the mean of normalized FLuc values of three agroinfiltrated leaves (n=3) ± SD. Statistical analysis were performed using unpaired t-test, P-Value ≤ 0.05.